<u>ATTACHMENT 2</u>

CDI REPORT 09-26NP (NON-PROPRIETARY)

STRESS ASSESSMENT OF NINE MILE POINT UNIT 2 STEAM DRYER AT CLTP AND EPU CONDITIONS, REV. 0

Nine Mile Point Nuclear Station, LLC
August 28, 2009

This Document Does Not Contain Continuum Dynamics, Inc. Proprietary Information

CDI Report No. 09-26NP

Stress Assessment of Nine Mile Point Unit 2 Steam Dryer at CLTP and EPU Conditions

Revision 0

Prepared by

Continuum Dynamics, Inc.
34 Lexington Avenue
Ewing, NJ 08618

Prepared under Purchase Order No. 7708631 for

Constellation Energy Group
Nine Mile Point Nuclear Station, LLC
P. O. Box 63
Lycoming, NY 13093

Approved by

Alan J. Bilanin

Reviewed by

Milton E. Teske

August 2009

This report complies with Continuum Dynamics, Inc. Nuclear Quality Assurance Program currently in effect.

Executive Summary

The finite element model and analysis methodology, used to assess stresses induced by the flow of steam through the steam dryer at Nine Mile Point Unit 2 (NMP2), are described and applied to obtain stresses at CLTP conditions. The analysis is consistent with those carried out in the U.S. for dryer qualification to EPU conditions and complies with a standard analysis procedure [1] supported by the EPRI BWRVIP and currently under review by the USNRC. The resulting stresses are assessed for compliance with the ASME B&PV Code 2007 [2], Section III, subsection NG, for the load combination corresponding to normal operation (the Level A Service Condition).

The analysis is carried out in the frequency domain, which confers a number of useful computational advantages over a time-accurate transient analysis including the ability to assess the effects of frequency scaling in the loads without the need for additional finite element calculations. [[

(3)]] The analysis develops a series of unit stress solutions corresponding to the application of a unit pressure at a MSL at specified frequency, f. Each unit solution is obtained by first calculating the associated acoustic pressure field using a separate analysis that solves the damped Helmholtz equation within the steam dryer [3]. This pressure field is then applied to a finite element structural model of the steam dryer and the harmonic stress response at frequency, f, is calculated using the commercial ANSYS 10.0 finite element analysis software. This stress response constitutes the unit solution and is stored as a file for subsequent processing. Once all unit solutions have been computed, the stress response for any combination of MSL pressure spectrums (obtained by Fast Fourier Transform of the pressure histories in the MSLs) is determined by a simple matrix multiplication of these spectrums with the unit solutions.

Results obtained from application of the methodology to the NMP2 steam dryer show that at nominal CLTP operation (no frequency shift) the minimum alternating stress ratio (SR-a) anywhere on the steam dryer is SR-a=3.00. The loads used to obtain this value account for all the end-to-end biases and uncertainties in the loads model [4] and finite element analysis. It is noted that:

(i) The signals account for the revised biases and uncertainties in the 60-70 Hz and 70-100 Hz frequency ranges. For various reasons the ACM was not recalibrated over the new frequency ranges (such a recalibration is resource-intensive and would lead to a new revision of the ACM). As a result, the biases and uncertainties in the new intervals are overly conservative and higher than they would otherwise be, had such a recalibration of the ACM been performed.

(ii) It is known that the signals used to estimate acoustic loads contain significant non-acoustic contributions referred to collectively as plant noise (e.g., pipe vibrations). However, to expedite qualification, <u>no noise removal has been performed for the analyses contained herein</u>.

Both of these load details increase conservatism in the analysis. Moreover, to account for uncertainties in the modal frequency predictions of the finite element model, the stresses are also computed for loads that are shifted in the frequency domain by ±2.5%, ±5%, ±7.5% and ±10%. The minimum alternating stress ratio encountered at any frequency shift is found to be SR-a=2.89 occurring at the -5% shift. The stress ratio due to maximum stresses (SR-P) is dominated by static loads and is SR-P=1.34 both with and without frequency shifts.

Since flow-induced acoustic resonances are not anticipated in the steam dryer, the alternating stress ratios at EPU operation can be obtained by scaling the CLTP values by the steam flow velocity squared, $(U_{EPU}/U_{CLTP})^2=1.178^2=1.388$. Under this approach, the limiting alternating stress ratio becomes SR-a=2.89/1.388=2.08. Given that the alternating stress ratio SR-a obtained at EPU remains above 2.08 at all frequency shifts together with the comparatively small dependence of SR-P upon acoustic loads, the Unit 2 dryer is expected to qualify at EPU conditions.

In order to achieve these stress ratios, the closure plate requires modification and welds on the lifting rod braces require reinforcement. For the closure plates reinforcement strips are added to stiffen the closure plates. Also, the top 18 inches of the welds connecting the closure plates to the vane banks and to the hoods are reinforced by adding a weld on the inner side of the closure plate. For the lifting rod braces, increasing the weld size from 1/4 in to 1/2 in meets the target stress ratio.

Table of Contents

1. Introduction and Purpose

Plans to qualify the Nine Mile Point nuclear plant for operation at Extended Power Uprate (EPU) operating condition require an assessment of the steam dryer stresses experienced under the increased loads. The steam dryer loads due to pressure fluctuations in the main steam lines (MSLs) are potentially damaging and the cyclic stresses from these loads can produce fatigue cracking if loads are sufficiently high. The industry has addressed this problem with physical modifications to the dryers, as well as a program to define steam dryer loads and their resulting stresses. The purpose of the stress analysis discussed here is to calculate the maximum and alternating stresses generated during Current Licensed Thermal Power (CLTP) and Extended Power Uprate (EPU) and to determine the margins that exist when compared to stresses that comply with the ASME Code (ASME B&PV Code, Section III, subsection NG).

The stress analysis of the modified NMP2 steam dryer establishes whether the existing and proposed modifications are adequate for sustaining structural integrity and preventing future weld cracking under planned EPU operating conditions. The load combination considered here corresponds to normal operation (the Level A Service Condition) and includes fluctuating pressure loads developed from NMP2 main steam line data, and weight. The fluctuating pressure loads, induced by the flowing steam, are predicted using a separate acoustic circuit analysis of the steam dome and main steam lines [5]. Level B service conditions, which include seismic loads, are not included in this evaluation.

[[

(3)]] This approach also affords a number of additional computational advantages over transient simulations including: [[

(3)]] This last advantage is realized through the use of "unit" solutions representing the stress distribution resulting from the application of a unit fluctuating pressure at one of the MSLs at a particular frequency. [[
(3)]]

This report describes the overall methodology used to obtain the unit solutions in the frequency domain and how to assemble them into a stress response for a given combination of pressure signals in the MSLs. This is followed by details of the NMP2 steam dryer finite element model including the elements used and overall resolution, treatment of connections between elements, the hydrodynamic model, the implementation of structural damping and key idealizations/assumptions inherent to the model. Post-processing procedures are also reviewed including the computation of maximum and alternating stress intensities, identification of high stress locations, adjustments to stress intensities at welds and evaluation of stress ratios used to establish compliance with the ASME Code. The results in terms of stress intensity distributions and stress ratios are presented next together with PSDs of the dominant stress components.

In order to meet target EPU stress levels (i.e., an alternating stress ratio of 2.0), two components required modification: the closure plate welds and the lifting rod support braces. In the former case, stiffening strips or ribs are added to the closure plate to simultaneously increase the frequency and lower stresses [6]; also the closure plate attachment weld is strengthened by placing an additional weld on the interior side of the junction where the closure plate meets the hood or vane bank. For the lifting rod braces, the existing 1/4 in weld is increased to 1/2 in. Both modifications involve the use of highly detailed solid element-based sub-models of these locations to accurately assess the local stresses.

2. Methodology

2.1 Overview

Based on previous analysis undertaken at Quad Cities Units 1 and 2, the steam dryer can experience strong acoustic loads due to the fluctuating pressures in the MSLs connected to the steam dome containing the dryer. C.D.I. has developed an acoustic circuit model (ACM) that, given a collection of strain gage measurements [7] of the fluctuating pressures in the MSLs, predicts the acoustic pressure field anywhere inside the steam dome and on the steam dryer [1, 3-5]. The ACM is formulated in frequency space and contains two major components that are directly relevant to the ensuing stress analysis of concern here. [[

(3)]]

[[

[3]]]

[[

(3)]]

2.2 [[(3)]]

[[

(3)]]

[[

(3)]]

2.3 Computational Considerations

Focusing on the structural computational aspects of the overall approach, there are a number of numerical and computational considerations requiring attention. The first concerns the transfer of the acoustic forces onto the structure, particularly the spatial and frequency resolutions. The ANSYS finite element program inputs general distributed pressure differences using a table format. This consists of regular 3D rectangular (i.e., block) $n_x \times n_y \times n_z$ mesh where n_α is the number of mesh points in the i-th Cartesian direction and the pressure difference is provided at each mesh point (see Section 3.10). These tables are generated separately using a program that reads the loads provided from the ACM software, distributes these loads onto the finite element mesh using a combination of interpolation procedures on the surface and simple diffusion schemes off the surface (off-surface loads are required by ANSYS to ensure proper interpolation of forces), and written to ASCII files for input to ANSYS. A separate load file is written at each frequency for the real and imaginary component of the complex force.

The acoustic field is stored at 5 Hz intervals from 0 to 250 Hz. While a 5 Hz resolution is sufficient to capture frequency dependence of the acoustic field (i.e., the pressure at a point varies gradually with frequency), it is too coarse for representing the structural response especially at low frequencies. For 1% critical structural damping, one can show that the frequency spacing needed to resolve a damped resonant peak at natural frequency, f_n, to within 5% accuracy is $\Delta f = 0.0064 \times f_n$. Thus for $f_n = 10$ Hz where the lowest structural response modes occur, a frequency interval of 0.064 Hz or less is required. In our calculations we require that 5% maximum error be maintained over the range from $f_n = 5$ Hz to 250 Hz resulting in a finest frequency interval of 0.0321 Hz at the low frequency end (this adequately resolves all structural modes up to 250 Hz). Since there are no structural modes between 0 to 5 Hz, a 0.5 Hz spacing is used over this range with minimal (less than 5%) error. The unit load, $\hat{\mathbf{f}}_n(\omega, \mathbf{R})$, at any frequency, ω_k, is obtained by linear interpolation of the acoustic solutions at the two nearest frequencies, ω_i and ω_{i+1}, spaced 5 Hz apart. Linear interpolation is sufficient since the pressure load varies slowly over the 5 Hz range (linear interpolation of the structural response would not be acceptable over this range since it varies much more rapidly over the same interval). Details regarding the frequency resolution have been provided in [9].

Solution Management

[[

(3)]]

[[

(3)]]

Structural Damping

In harmonic analysis one has a broader selection of damping models than in transient simulations. A damping factor, z, of 1% critical damping is used in the structural analysis. In transient simulations, this damping can only be enforced exactly at two frequencies (where the damping model is "pinned"). Between these two frequencies the damping factor can by considerably smaller, for example 0.5% or less depending on the pinning frequencies. Outside the pinning frequencies, damping is higher. With harmonic analysis it is straightforward to enforce very close to 1% damping over the entire frequency range. In this damping model, the damping matrix, **D**, is set to

$$\mathbf{D} = \frac{2z}{\omega}\mathbf{K} \tag{7}$$

where **K** is the stiffness matrix and ω the forcing frequency. When comparing the response obtained with this model against that for a constant damping ratio, the maximum difference at any frequency is less than 0.5%, which is far smaller than the 100% or higher response variation obtained when using the pinned model required in transient simulation.

Load Frequency Rescaling

One way to evaluate the sensitivity of the stress results to approximations in the structural modeling and applied loads is to rescale the frequency content of the applied loads. In this procedure the nominal frequencies, ω_k, are shifted to $(1+\lambda)\omega_k$, where the frequency shift, λ, ranges between $\pm 10\%$, and the response recomputed for the shifted loads. The objective of the frequency shifting can be explained by way of example. Suppose that in the actual dryer a strong structural-acoustic coupling exists at a particular frequency, ω^*. This means that the following conditions hold simultaneously: (i) the acoustic signal contains a significant signal at ω^*; (ii) the structural model contains a resonant mode of natural frequency, ω_n, that is near ω^*; and (iii) the associated structural mode shape is strongly coupled to the acoustic load (i.e., integrating the product of the mode shape and the surface pressure over the steam dryer surface produces a significant modal force). Suppose now that because of discretization errors and modeling idealizations that the predicted resonance frequency differs from ω^* by a small amount (e.g., 1.5%). Then condition (ii) will be violated and the response amplitude therefore significantly diminished. By shifting the load frequencies one re-establishes condition (ii) when $(1+\lambda)\omega^*$ is near ω_n. The other two requirements also hold and a strong structural acoustic interaction is restored.

[[

(3)]]

Evaluation of Maximum and Alternating Stress Intensities

Once the unit solutions have been obtained, the most intensive computational steps in the generation of stress intensities are: (i) the FFTs to evaluate stress time histories from (5); and (ii) the calculation of alternating stress intensities. [[

(3)]]

The high computational penalty incurred in calculating the alternating stress intensities is due to the fact that this calculation involves comparing the stress tensors at every pair of points in the stress history. This comparison is necessary since in general the principal stress directions can vary during the response, thus for N samples in the stress history, there will be (N-1)N/2 such pairs or, for N=64K (the number required to accurately resolve the spectrum up to 250 Hz in 0.01 Hz intervals), 2.1×10^9 calculations per node each requiring the determination of the roots to a cubic polynomial. [[

(3)]]

3. Finite Element Model Description

A description of the ANSYS model of the nine Mile Point Unit 2 steam dryer follows.

3.1 Steam Dryer Geometry

A geometric representation of the Nine Mile Point Unit 2 steam dryer was developed from available drawings (provided by Constellation Energy Group and included in the design record file, DRF-C-279C) within the Workbench module of ANSYS. The completed model is shown in Figure 1. This model includes on-site modifications to the Nine Mile Point Unit 2 steam dryer. These are as follows.

On-Site Modifications

(i) The top tie rods are replaced with thicker ones.
(ii) Inner side plates are replaced with thicker ones.
(iii) Middle hoods are reinforced with additional strips.
(iv) Lifting rods are reinforced with additional gussets.
(v) Per FDDR KG1-0265 the support conditions are adjusted to ensure that the dryer is supported 100% on the seismic blocks.

These additional modifications have been incorporated into the NMP2 steam dryer model and are reflected in the results presented in this report. The affected areas are shown in Figure 2.

Modifications Planned for EPU Operation

To meet the target stress ratio at EPU, reinforcement of the closure plates and increases in selected weld sizes are recommended. Analysis shows that the original closure plates experience a strong response from forcing of one of its structural modes. These structures have been modified using stiffening strips to simultaneously reinforce them and shift their frequencies away from significant acoustic loads [6]. Analysis of these components is summarized in Appendix A. Modifications to welds are analyzed using sub-models to minimize computational cost. These analyses are performed at the following locations as discussed further in Section 4.5: (i) the lifting rod support braces; (ii) closure plate welds and (iii) the ends of selected tie bars. In addition, previous analyses of geometrically identical and similarly loaded locations have been applied at these locations and in the locations where reinforcements are implemented.

Reference Frame

The spatial coordinates used herein to describe the geometry and identify limiting stress locations are expressed in a reference frame whose origin is located at the intersection of the steam dryer centerline and the plane containing the base plates (this plane also contains the top of the upper support ring and the bottom edges of the hoods). The y-axis is parallel to the hoods, the x-axis is normal to the hoods pointing from MSL C/D to MSL A/B, and the z-axis is vertical, positive up.

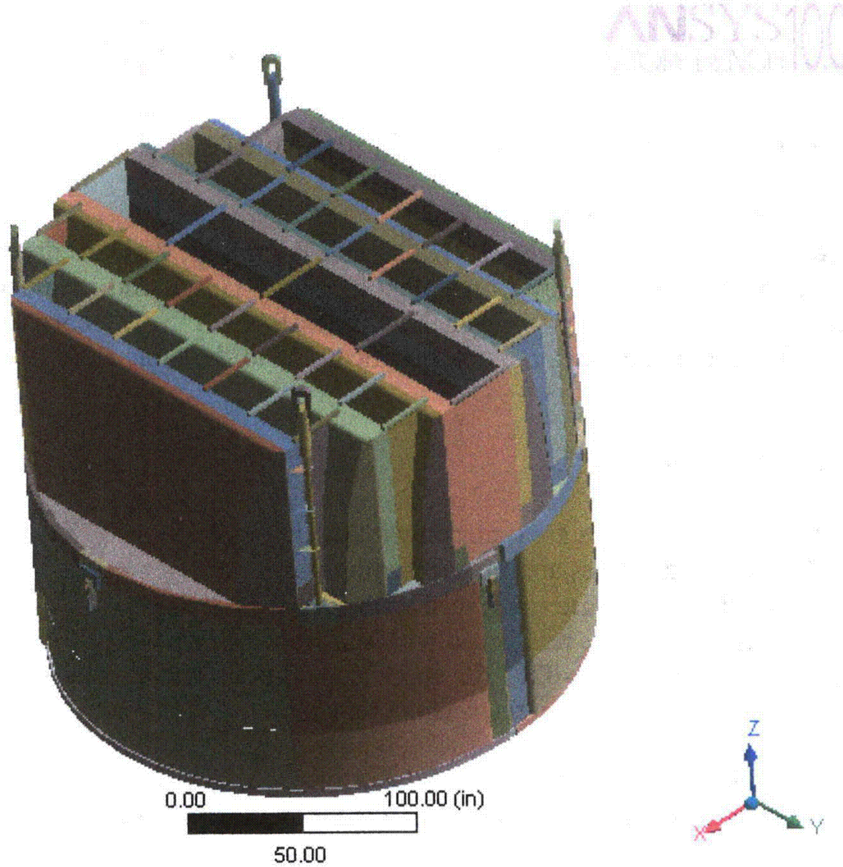

Figure 1. Overall geometry of the Nine Mile Point Unit 2 steam dryer model.

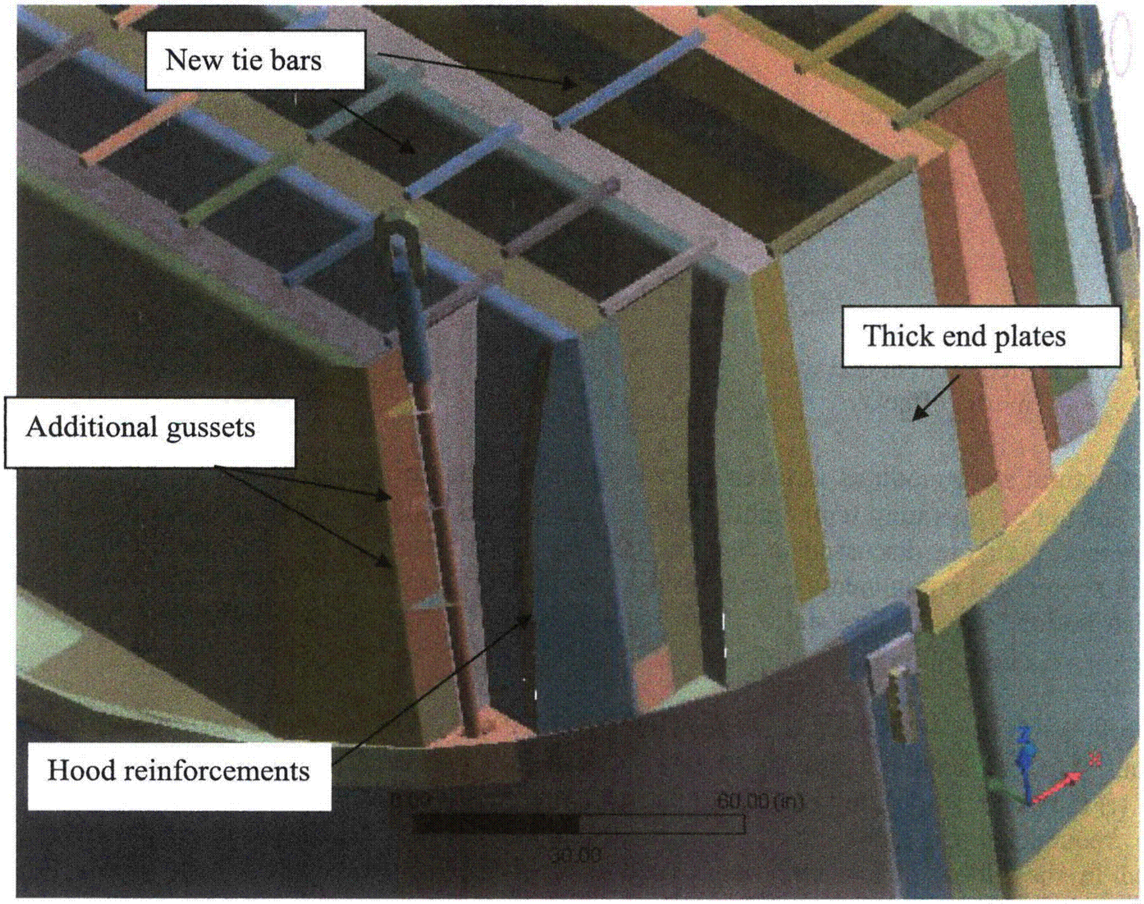

Figure 2. Modify the figure to eliminate inner hood strips. On-site modifications accounted for in the model and associated geometrical details.

3.2 Material Properties

The steam dryer is constructed from Type 304 stainless steel and has an operating temperature of 550°F. Properties used in the analysis are summarized below in Table 1.

Table 1. Material properties.

	Young's Modulus (10^6 psi)	Density (lbm/in^3)	Poisson Ratio
stainless steel	25.55	0.284	0.3
structural steel with added water inertia effect	25.55	0.856	0.3

The structural steel modulus is taken from Appendix A of the ASME Code for Type 304 Stainless Steel at an operating temperature 550°F. The effective properties of perforated plates and submerged parts are discussed in Sections 3.4 and 3.6. Note that the increased effective density for submerged components is only used in the harmonic analysis. When calculating the stress distribution due to the static dead weight load, the unmodified density of steel (0.284 lbm/in^3) is used throughout.

Inspections of the NMP Unit 2 dryer have revealed IGSCC cracks in the upper support ring (USR) and skirt. A separate analysis of these cracks [12] has been performed to determine whether: (i) they will propagate further into the structure and (ii) their influence upon structural response frequencies and modes must be explicitly accounted for. To establish (i) the stress calculated in the global stress analysis is used in conjunction with the crack geometry to calculate the stress intensity factor which is then compared to the threshold stress intensity. For the USR and skirt cracks the highest stress intensity factors are 1.47 ksi-$in^{0.5}$ and 2.75 ksi-$in^{0.5}$ respectively; both values are below the threshold value (3 ksi-$in^{0.5}$) implying that fatigue crack growth will not occur.

To determine (ii) the change in modal response frequencies due to the presence of a flaw is predicted by analytical means (in the case of the USR) or using finite element analysis (for the skirt). In each case, the flaw size used in these calculations is increased to ensure conservative estimates (for example, in the case of the skirt flaws extending up to ½ the panel width are considered). For the USR, the change in modal frequencies due to the presence of the cracks is less than 0.5%. For the skirt, using a conservative estimate for the crack to panel width of 0.3 (the measured value is less than 0.17) the change in modal frequency is also less than 0.5%. In both cases such small changes in modal frequencies are considers negligible and are readily accounted for when performing frequency shifting.

3.3 Model Simplifications

The following simplifications were made to achieve reasonable model size while maintaining good modeling fidelity for key structural properties:

- Perforated plates were approximated as continuous plates using modified elastic properties designed to match the static and modal behaviors of the perforated plates. The perforated plate structural modeling is summarized in Section 3.4 and Appendix C of [13].

- The drying vanes were replaced by point masses attached to the corresponding trough bottom plates and vane bank top covers (Figure 4). The bounding perforated plates, vane bank end plates, and vane bank top covers were explicitly modeled (see Section 3.5).

- The added mass properties of the lower part of the skirt below the reactor water level were obtained using a separate hydrodynamic analysis (see Section 3.6).

- [[(3)]]

- Four steam dryer support brackets that are located on the reactor vessel and spaced at 90° intervals were explicitly modeled (see Section 3.9).

- Most welds were replaced by node-to-node connections; interconnected parts share common nodes along the welds. In other locations the constraint equations between nodal degrees of freedom were introduced as described in Section 3.9.

3.4 Perforated Plate Model

The perforated plates were modeled as solid plates with adjusted elastic and dynamic properties. Properties of the perforated plates were assigned according to the type and size of perforation. Based on [14], for an equilateral square pattern with given hole size and spacing, the effective moduli of elasticity were found.

The adjusted properties for the perforated plates are shown in Table 2 as ratios to material properties of structural steel, provided in Table 1. Locations of perforated plates are classified by steam entry / exit vane bank side and vertical position.

Tests were carried out to verify that this representation of perforated plates by continuous ones with modified elastic properties preserves the modal properties of the structure. These tests are summarized in Appendix C of [13]and compare the predicted first modal frequency for a cantilevered perforated plate against an experimentally measured value. The prediction was obtained for 40% and 13% open area plates (these are representative of the largest and lowest open area ratios of the perforated plates at NMP2, as seen in Table 2) using the analytical formula for a cantilevered plate and the modified Young's modulus and Poisson's ratio given by O'Donnell [14]. The measured and predicted frequencies are in close agreement, differing by less than 3%.

[[(3)]]

[[

[3]]].

[[

[3]]]

Figure 3. [[

[3]]]

Table 2. Material properties of perforated plates.

[[

(3)]]

3.5 Vane Bank Model

The vane bank assemblies consist of many vertical angled plates that are computationally expensive to model explicitly, since a prohibitive number of elements would be required. These parts have significant weight which is transmitted through the surrounding structure, so it is important to capture their gross inertial properties. Here the vane banks are modeled as a collection of point masses located at the center of mass for each vane bank section (Figure 4). The following masses were used for the vane bank sections, based on data found on provided drawings:

inner banks, 1618 lbm, 4 sections per bank;
middle banks, 1485 lbm, total 4 sections per bank; and
outer banks, 1550 lbm, 3 sections per bank.

These masses were applied to the base plates and vane top covers using the standard ANSYS point mass modeling option, element MASS21. ANSYS automatically distributes the point mass inertial loads to the nodes of the selected structure. The distribution algorithm minimizes the sum of the squares of the nodal inertial forces, while ensuring that the net forces and moments are conserved. Vane banks are not exposed to main steam lines directly, but rather shielded by the hoods.

The collective stiffness of the vane banks is expected to be small compared to the surrounding support structure and is neglected in the model. In the static case it is reasonable to expect that this constitutes a conservative approach, since neglecting the stiffness of the vane banks implies that the entire weight is transmitted through the adjacent vane bank walls and supports. In the dynamic case the vane banks exhibit only a weak response since (i) they have large inertia so that the characteristic acoustically-induced forces divided by the vane masses and inertias yield small amplitude motions, velocities and accelerations; and (ii) they are shielded from acoustic loads by the hoods, which transfer dynamic loads to the rest of the structure. Thus, compared to the hoods, less motion is anticipated on the vane banks so that approximating their inertial properties with equivalent point masses is justified. Nevertheless, the bounding parts, such as perforated plates, side panels, and top covers, are retained in the model. Errors associated with the point mass representation of the vane banks are compensated for by frequency shifting of the applied loads.

3.6 Water Inertia Effect on Submerged Panels

Water inertia was modeled by an increase in density of the submerged structure to account for the added hydrodynamic mass. This added mass was found by a separate hydrodynamic analysis (included in DRF-C-279C supporting this report) to be 0.143 lbm/in^2 on the submerged skirt area. This is modeled by effectively increasing the material density for the submerged portions of the skirt. Since the skirt is 0.25 inches thick, the added mass is equivalent to a density increase by 0.572 lbm/in^3. This added water mass was included in the ANSYS model by appropriately modifying the density of the submerged structural elements when computing harmonic response. For the static stresses, the unmodified density of steel is used throughout.

3.7 Structural Damping

Structural damping was defined as 1% of critical damping for all frequencies. This damping is consistent with guidance given on pg. 10 of NRC RG-1.20 [18].

3.8 Mesh Details and Element Types

Shell elements were employed to model the skirt, hoods, perforated plates, side and end plates, trough bottom plates, reinforcements, base plates and cover plates. Specifically, the four-node, Shell Element SHELL63, was selected to model these structural components. This element models bending and membrane stresses, but omits transverse shear. The use of shell elements is appropriate for most of the structure where the characteristic thickness is small compared to the other plate dimensions. For thicker structures, such as the upper and lower support rings, solid brick elements were used to provide the full 3D stress. The elements SURF154 are used to assure proper application of pressure loading to the structure. Mesh details and element types are shown in Table 3 and Table 4.

The mesh is generated automatically by ANSYS with refinement near edges. The maximum allowable mesh spacing is specified by the user. Here a 2.5 inch maximum allowable spacing is specified with refinement up to 1.5 inch in the following areas: drain pipes, tie rods, the curved portions of the drain channels and the hoods. Details of the finite element mesh are shown in Figure 5. Numerical experiments carried out using the ANSYS code applied to simple analytically tractable plate structures with dimensions and mesh spacings similar to the ones used for the steam dryer, confirm that the natural frequencies are accurately recovered (less than 1% errors for the first modes). These errors are compensated for by the use of frequency shifting.

3.9 Connections Between Structural Components

Most connections between parts are modeled as node-to-node connections. This is the correct manner (i.e., within the finite element framework) of joining elements away from discontinuities. At joints between shells, this approach omits the additional stiffness provided by the extra weld material. Also, locally 3D effects are more pronounced. The latter effect is accounted for using weld factors. The deviation in stiffness due to weld material is negligible, since weld dimensions are on the order of the shell thickness. The consequences upon modal frequencies and amplitude are, to first order, proportional to t/L where t is the thickness and L a characteristic shell length. The errors committed by ignoring additional weld stiffness are thus small and readily compensated for by performing frequency shifts.

When joining shell and solid elements, however, the problem arises of properly constraining the rotations, since shell element nodes contain both displacement and rotational degrees of freedom at every node whereas solid elements model only the translations. A node-to-node connection would effectively appear to the shell element as a simply supported, rather than (the correct) cantilevered restraint and significantly alter the dynamic response of the shell structure.

To address this problem, constraint equations are used to properly connect adjacent shell- and solid-element modeled structures. Basically, all such constraints express the deflection (and rotation for shell elements) of a node, $\mathbf{R}_1$, on one structural component in terms of the deflections/rotations of the corresponding point, $\mathbf{P}_2$, on the other connected component. Specifically, the element containing $\mathbf{P}_2$ is identified and the deformations at $\mathbf{P}_2$ determined by interpolation between the element nodes. The following types of shell-solid element connections are used in the steam dryer model including the following:

1. Connections of shell faces to solid faces (Figure 6a). While only displacement degrees of freedom are explicitly constrained, this approach also implicitly constrains the rotational degrees of freedom when multiple shell nodes on a sufficiently dense grid are connected to the same solid face.
2. Connections of shell edges to solids (e.g., connection of the bottom of closure plates with the upper ring). Since solid elements do not have rotational degrees of freedom, the coupling approach consisted of having the shell penetrate into the solid by one shell thickness and then constraining both the embedded shell element nodes (inside the solid) and the ones located on the surface of the solid structure (see Figure 6b). Numerical tests involving simple structures showed that this approach and penetration depth reproduce both the deflections and stresses of the same structure modeled using only solid elements or ANSYS' bonded contact technology. Continuity of rotations and displacements is achieved.

The use of constraint conditions rather than the bonded contacts advocated by ANSYS for connecting independently meshed structural components confers better accuracy and useful numerical advantages to the structural analysis of the steam dryer including better conditioned and smaller matrices. The smaller size results from the fact that equations and degrees of freedom are eliminated rather than augmented (in Lagrange multiplier-based methods) by additional degrees of freedom. Also, the implementation of contact elements relies on the use of very high stiffness elements (in penalty function-based implementations) or results in indefinite matrices (Lagrange multiplier implementations) with poorer convergence behavior compared to positive definite matrices.

The steam dryer rests on four support blocks which resist vertical and lateral displacement. The support blocks contact the seismic blocks welded to the USR so that 100% of the dryer weight is transmitted through the seismic blocks per the FDDR KG1-265. Because the contact region between the blocks and steam dryer is small, the seismic blocks are considered free to rotate about the radial axis. Specifically nodal constraints (zero relative displacement) are imposed over the contact area between the seismic blocks and the support blocks. Two nodes on each support block are fixed as indicated in Figure 7. One node is at the center of the support block surface facing the vessel and the other node is 0.5" offset inside the block towards the steam dryer, half way to the nearest upper support ring node. This arrangement approximates the nonlinear contact condition where the ring can tip about the block.

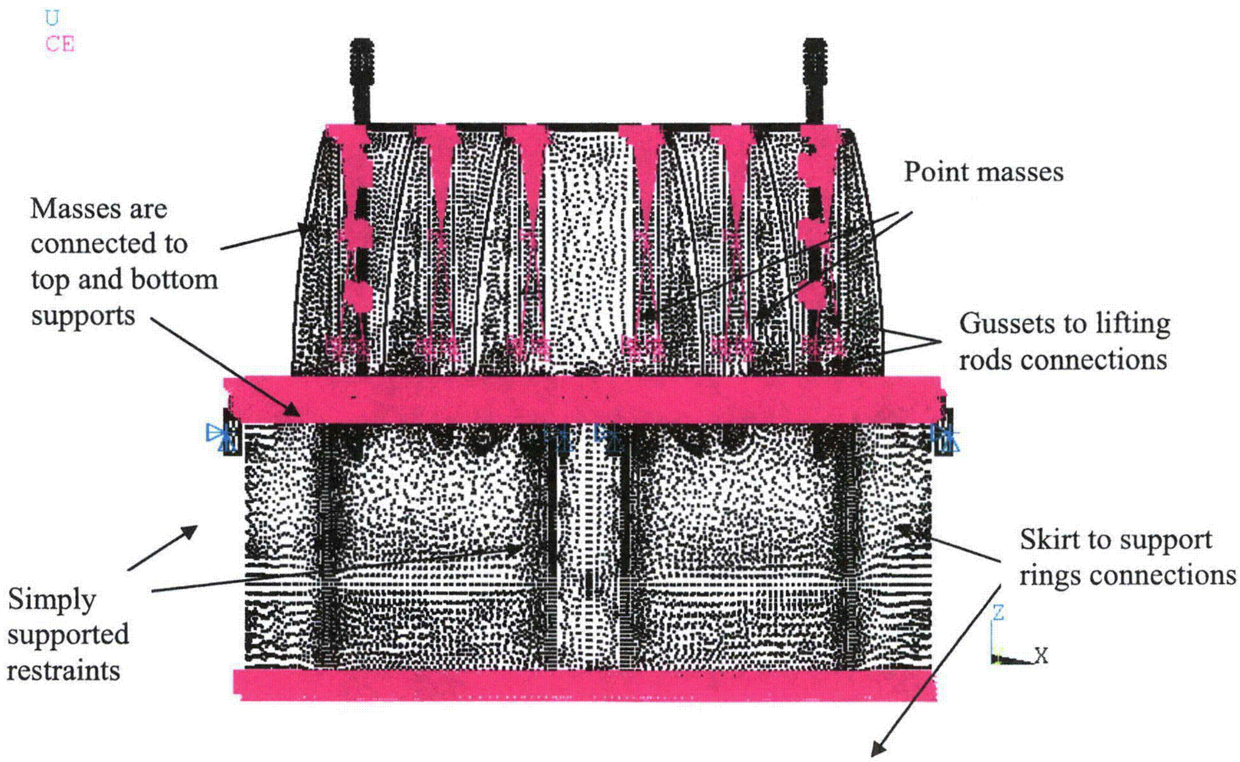

Figure 4. Point masses representing the vanes. The pink shading represents where constraint equations between nodes are applied (generally between solid and shell elements, point masses and nodes and [[(3)]]).

Table 3. FE Model Summary.

Description	Quantity
Total Nodes[1]	159,793
Total Elements	124,496

1. Not including additional damper nodes and elements.

Table 4. Listing of Element Types.

Generic Element Type Name	Element Name	ANSYS Name
20-Node Quadratic Hexahedron	SOLID186	20-Node Hexahedral Structural Solid
10-Node Quadratic Tetrahedron	SOLID187	10-Node Tetrahedral Structural Solid
4-Node Elastic Shell	SHELL63	4-Node Elastic Shell
Mass Element	MASS21	Structural Mass
Pressure Surface Definition	SURF154	3D Structural Surface Effect
Damper element	COMBIN14	Spring-Damper

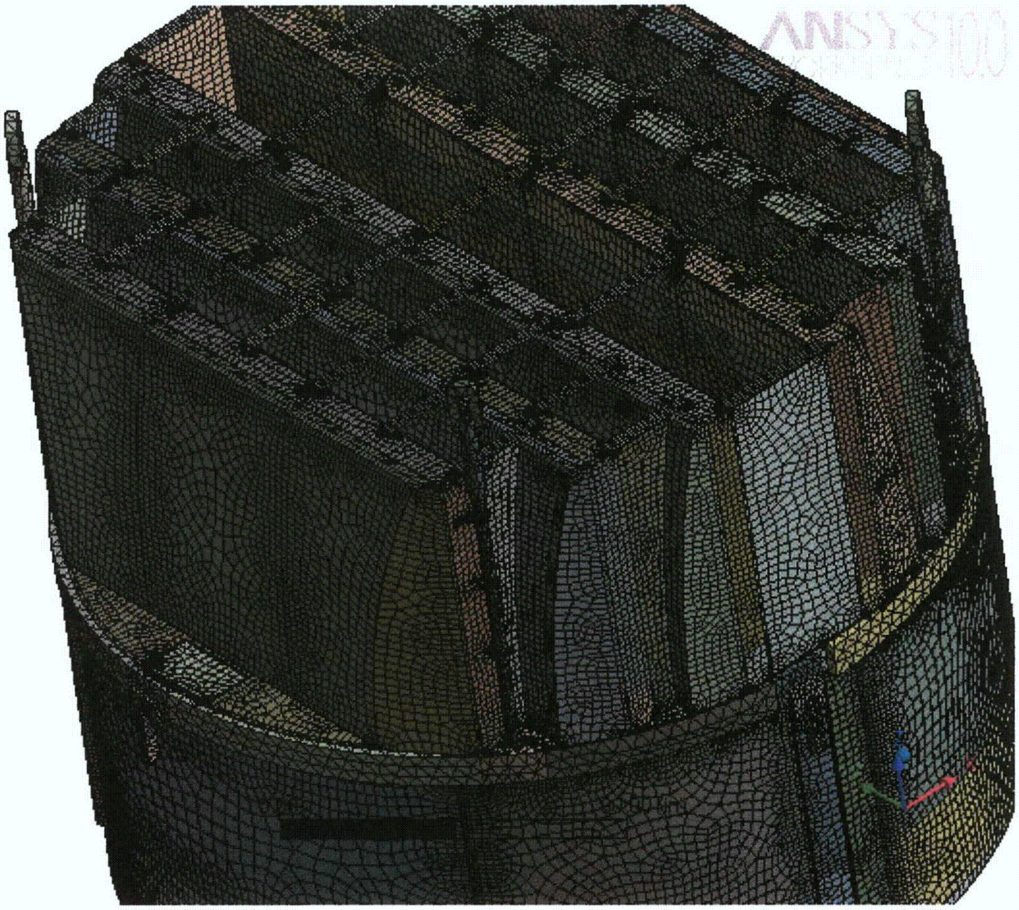

Figure 5a. Mesh overview.

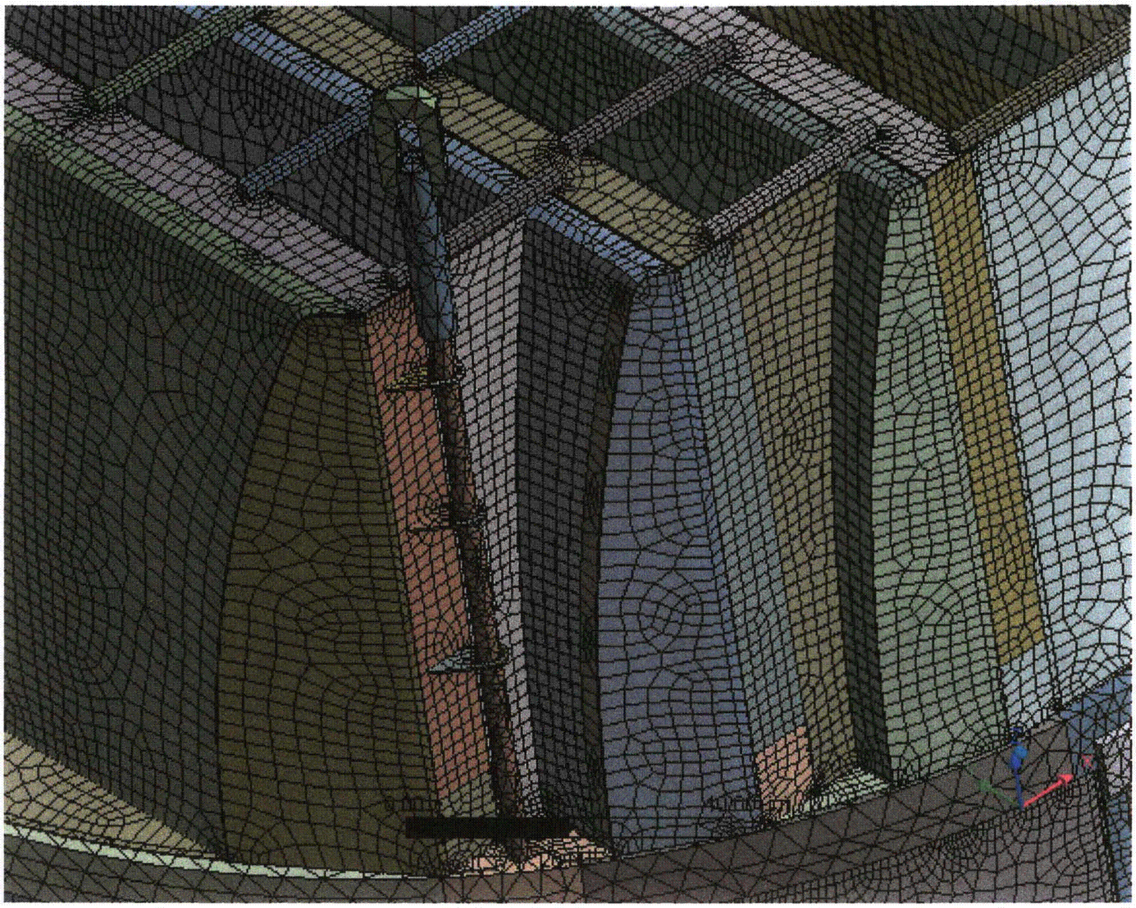

Figure 5b. Close up of mesh showing on-site modifications.

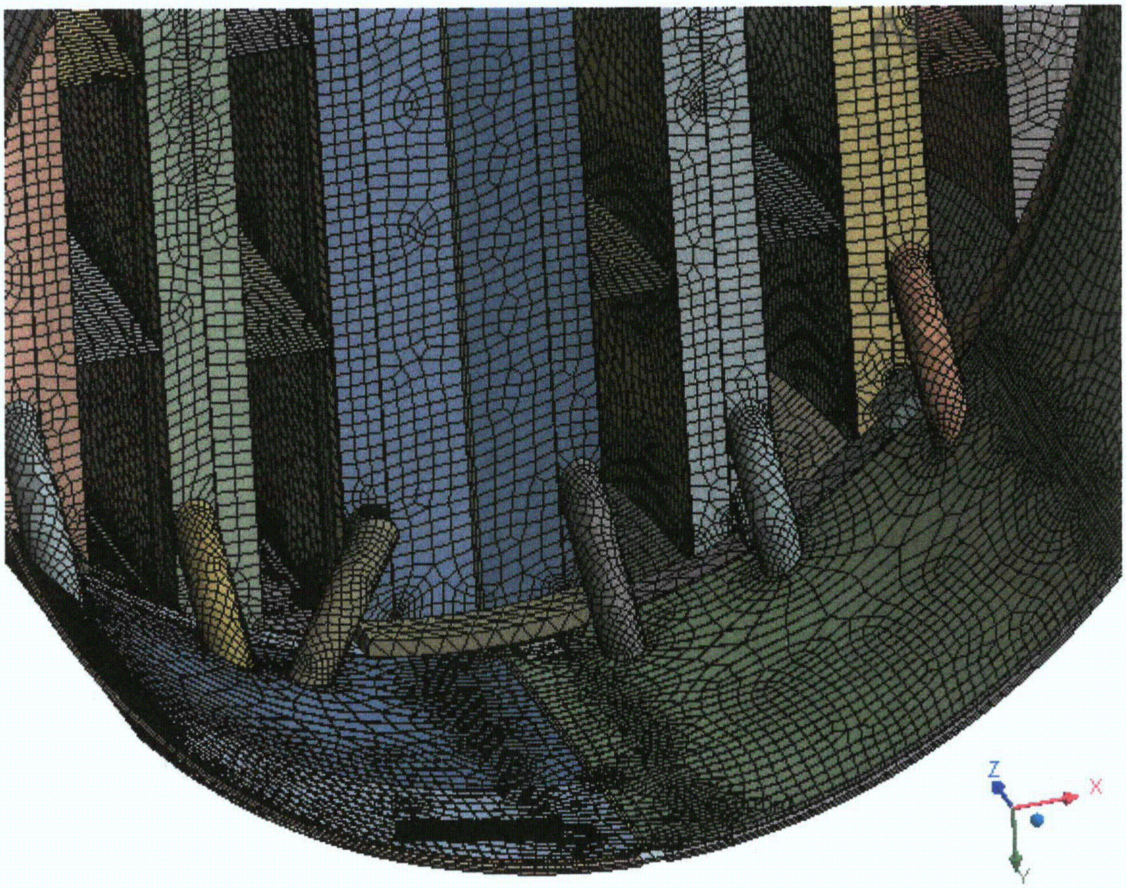

Figure 5c. Close up of mesh showing drain pipes and hood supports.

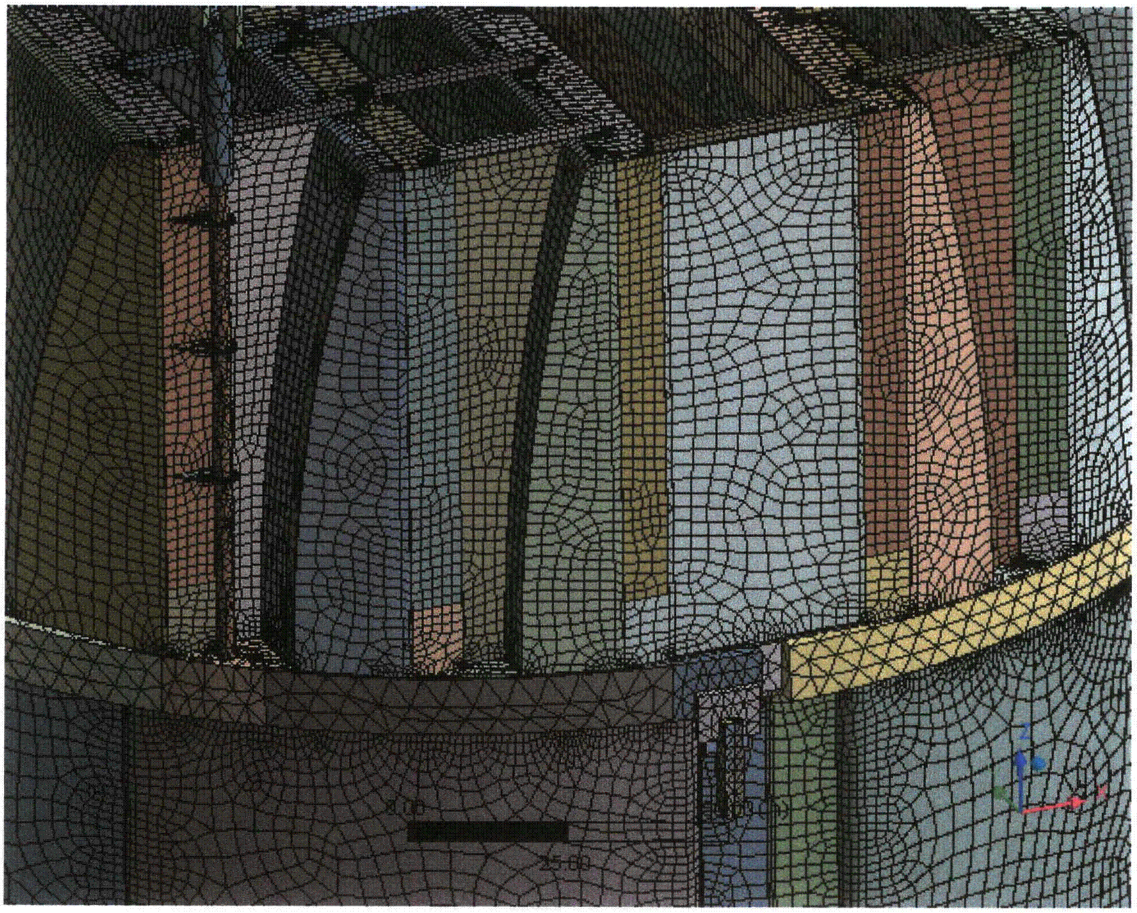

Figure 5d. Close up of mesh showing node-to-node connections between various plates.

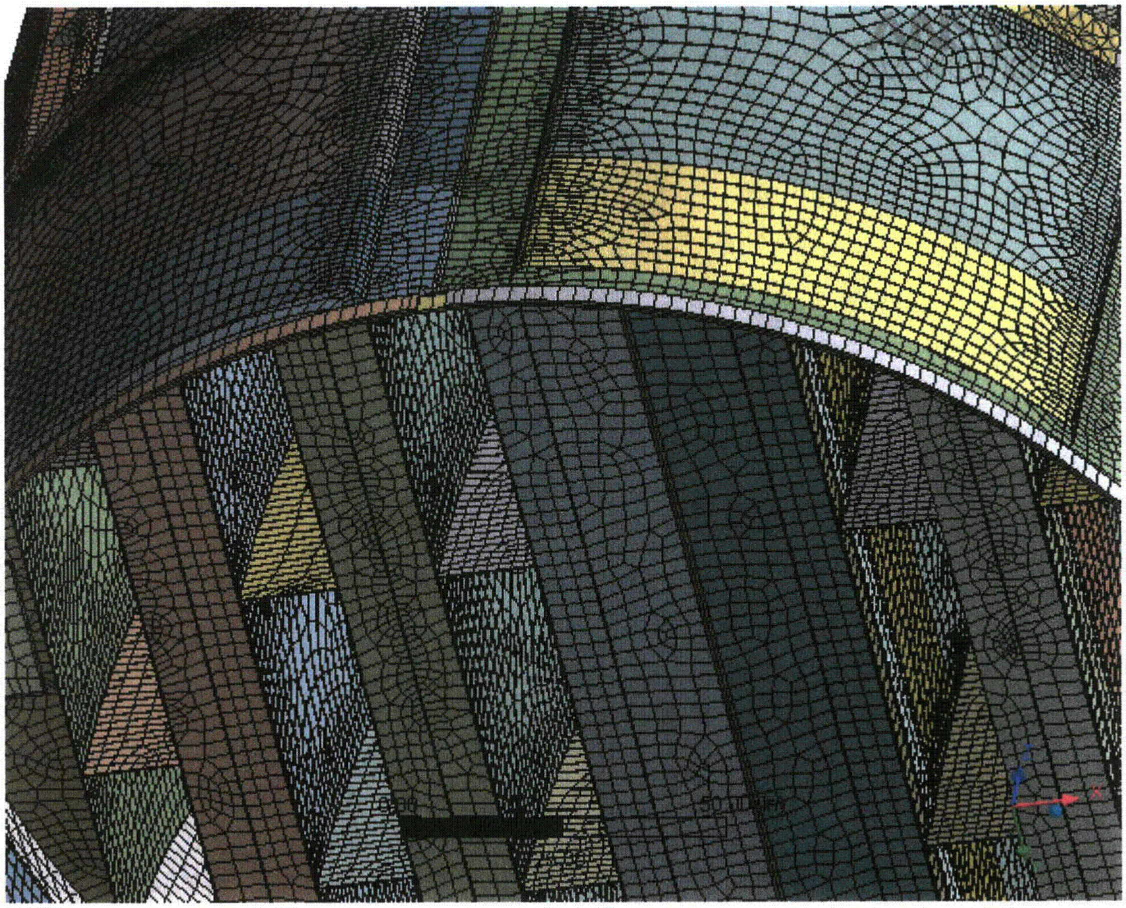

Figure 5e. Close up of mesh showing node-to-node connections between the skirt and drain channels; hood supports and hoods; and other parts.

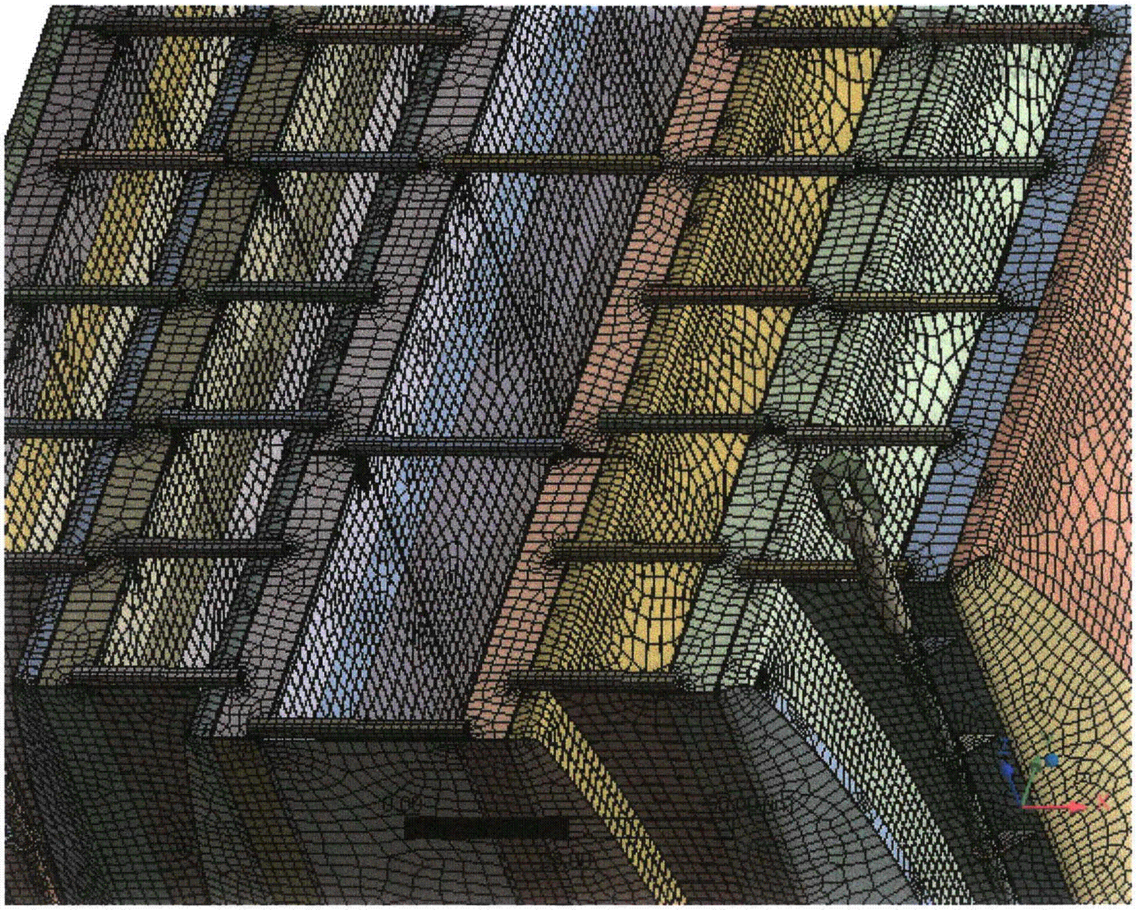

Figure 5f. Close up view of tie bars.

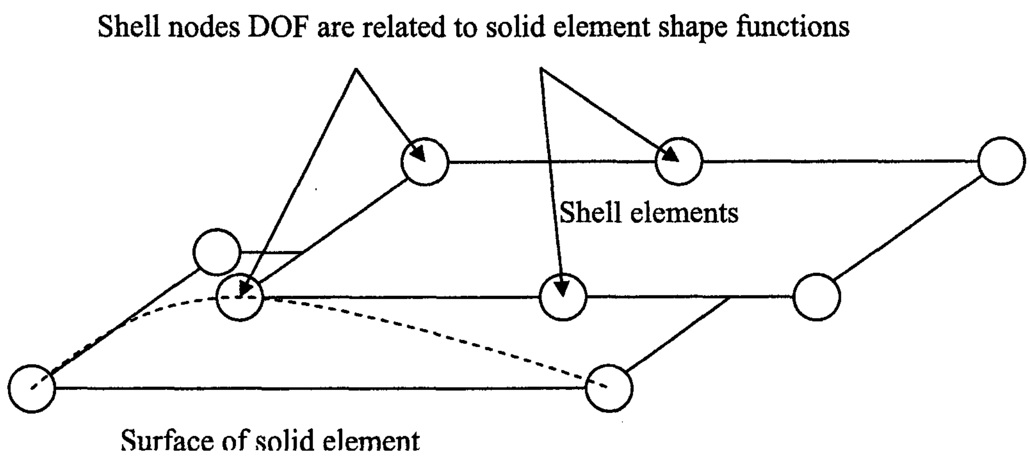

Figure 6a. Face-to-face shell to solid connection.

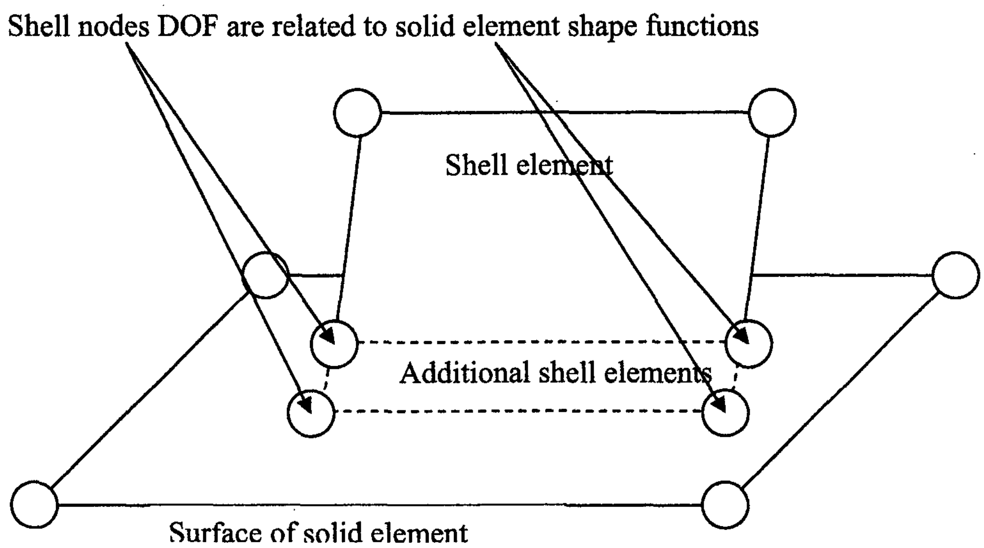

Figure 6b. Shell edge-to-solid face connection.

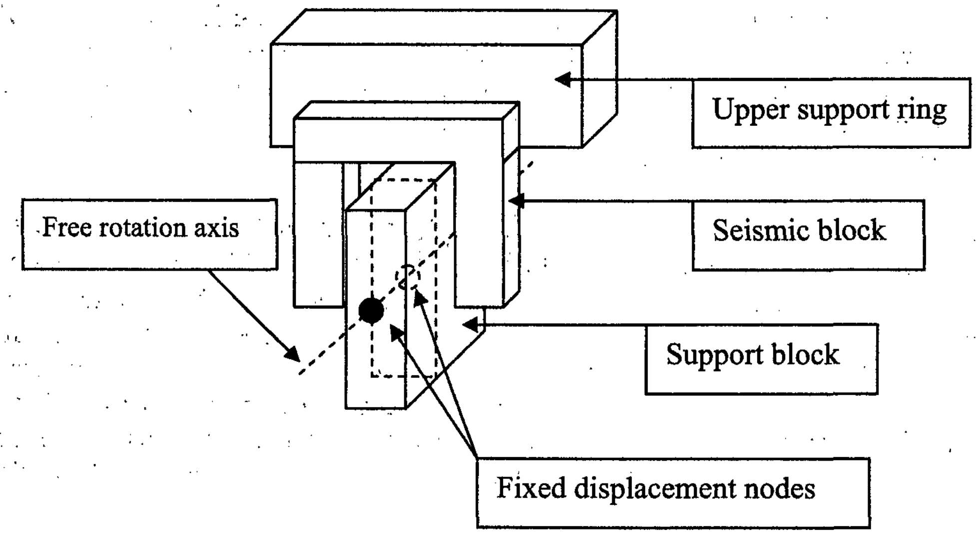

Figure 7. Boundary conditions. Inside node is half way between outer surface of support block and upper support ring.

3.10 Pressure Loading

The harmonic loads are produced by the pressures acting on the exposed surfaces of the steam dryer. At every frequency and for each MSL, the pressure distribution corresponding to a unit pressure at the MSL inlet is represented on a three-inch grid lattice grid (i.e., a mesh whose lines are aligned with the x-, y- and z-directions) that is superimposed over the steam dryer surface. This grid is compatible with the 'Table' format used by ANSYS to 'paint' general pressure distributions upon structural surfaces. The pressures are obtained from the Helmholtz solver routine in the acoustic analysis [3].

In general, the lattice nodes do not lie on the surface, so that to obtain the pressure differences at the surface it is necessary to interpolate the pressure differences stored at the lattice nodes. This is done using simple linear interpolation between the 8 forming nodes of the lattice cell containing the surface point of interest. Inspection of the resulting pressures at selected nodes shows that these pressures vary in a well-behaved manner between the nodes with prescribed pressures. Graphical depictions of the resulting pressures and comparisons between the peak pressures in the original nodal histories and those in the final surface load distributions produced in ANSYS, all confirm that the load data are interpolated accurately and transferred correctly to ANSYS.

The harmonic pressure loads are only applied to surfaces above the water level, as indicated in Figure 8. In addition to the pressure load, the static loading induced by the weight of the steam dryer is analyzed separately. The resulting static and harmonic stresses are linearly combined to obtain total values which are then processed to calculate maximum and alternating stress intensities for assessment in Section 5.

[[

(3)]] This is useful since revisions in the loads model do not necessitate recalculation of the unit stresses.

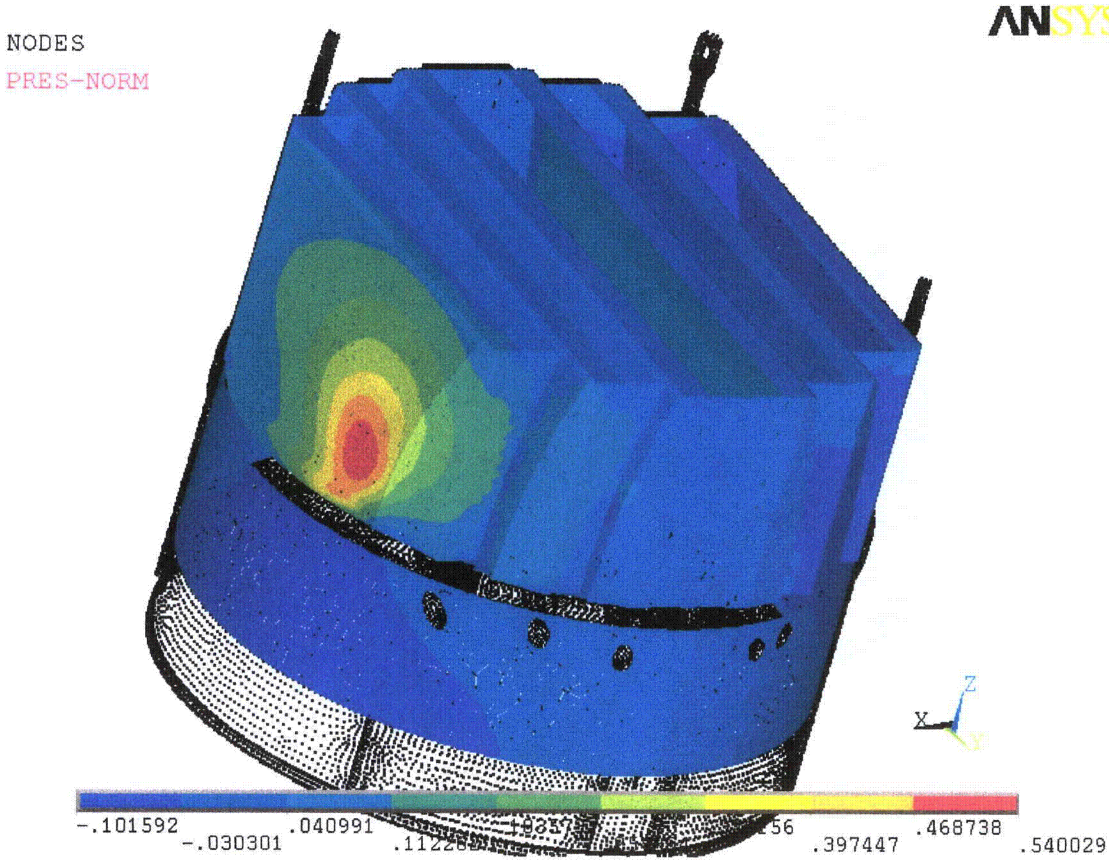

Figure 8a. Real part of unit pressure loading MSL A (in psid) on the steam dryer at 50.1 Hz. No loading is applied to the submerged surface and lifting rods.

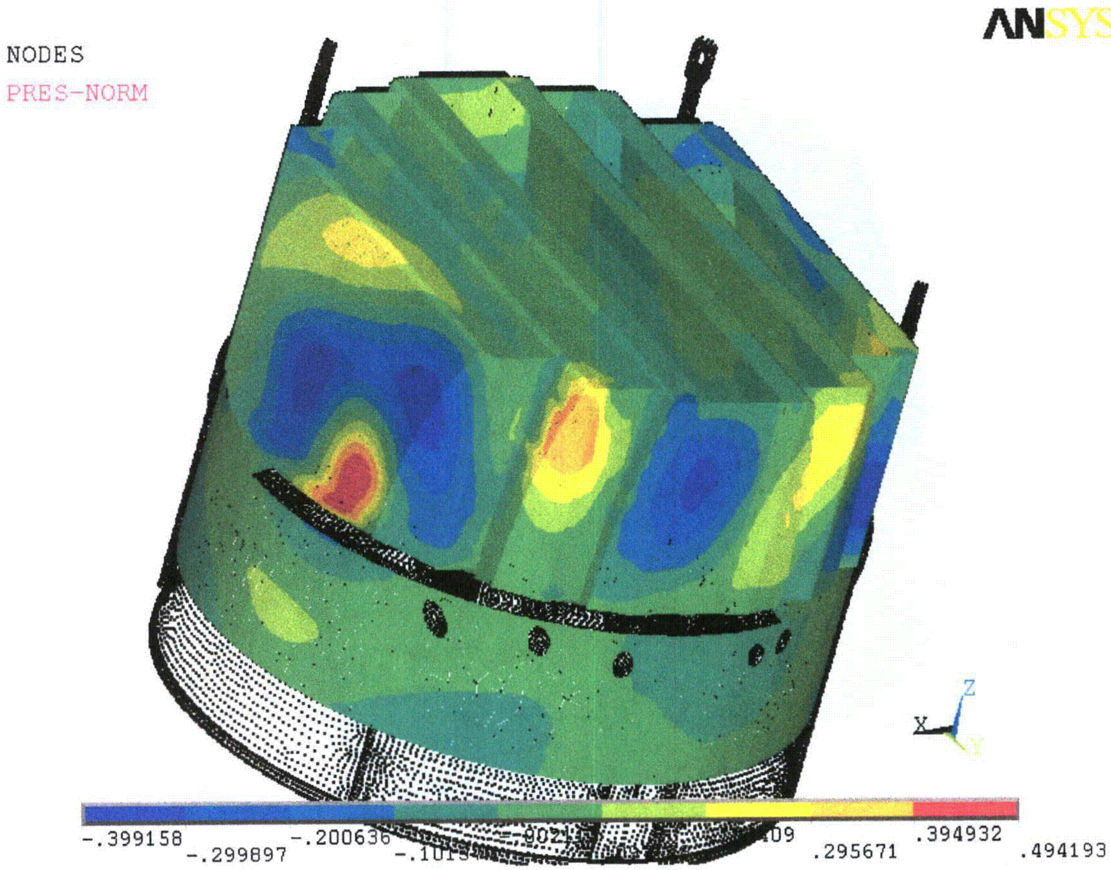

Figure 8b. Real part of unit pressure loading MSL A (in psid) on the steam dryer at 200.45 Hz. No loading is applied to the submerged surface and lifting rods.

4. Structural Analysis

The solution is decomposed into static and harmonic parts, where the static solution produces the stress field induced by the supported structure subjected to its own weight and the harmonic solution accounts for the harmonic stress field due to the unit pressure of given frequency in one of the main steam lines. All solutions are linearly combined, with amplitudes provided by signal measurements in each steam line, to obtain the final displacement and stress time histories. This decomposition facilitates the prescription of the added mass model accounting for hydrodynamic interaction and allows one to compare the stress contributions arising from static and harmonic loads separately. Proper evaluation of the maximum membrane and membrane+bending stresses requires that the static loads due to weight be accounted for. Hence both static and harmonic analyses are carried out.

4.1 Static Analysis

The results of the static analysis are shown in Figure 9. The locations with highest stress include the inner vane bank connection to inner base plate near support brackets with stress intensity 9,598 psi. There are four locations with artificial stress singularity, which are excluded from the analysis. The static stresses one node away are used at these locations as more realistic estimate of local stress. These locations are at the connections of the inner end plate to the inner base plate at the ends of the cut-out, as shown in Figure 9c.

4.2 Harmonic Analysis

The harmonic pressure loads were applied to the structural model at all surface nodes described in Section 3.10. Typical stress intensity distributions over the structure are shown in Figure 10. Stresses were calculated for each frequency, and results from static and harmonic calculations were combined.

To evaluate maximum stresses, the stress harmonics including the static component are transformed into a time history using FFT, and the maximum and alternating stress intensities for the response, evaluated. According to ASME B&PV Code, Section III, Subsection NG-3216.2 the following procedure was established to calculate alternating stresses. For every node, the stress difference tensors, $\boldsymbol{\sigma}'_{nm} = \boldsymbol{\sigma}_n - \boldsymbol{\sigma}_m$, are considered for all possible pairs of the stresses $\boldsymbol{\sigma}_n$ and $\boldsymbol{\sigma}_m$ at different time levels, t_n and t_m. Note that all possible pairs require consideration since there are no "obvious" extrema in the stress responses. However, in order to contain computational cost, extensive screening of the pairs takes place (see Section 2.3) so that pairs known to produce alternating stress intensities less than 500 psi are rejected. For each remaining stress difference tensor, the principal stresses S_1, S_2, S_3 are computed and the maximum absolute value among principal stress differences, $S_{nm} = \max\{|S_1 - S_2|, |S_1 - S_3|, |S_2 - S_3|\}$, obtained. The alternating stress at the node is then one-half the maximum value of S_{nm} taken over all combinations (n,m), i.e., $S_{alt} = \frac{1}{2}\max_{n,m}\{S_{nm}\}$. This alternating stress is compared against allowable values, depending on the node location with respect to welds.

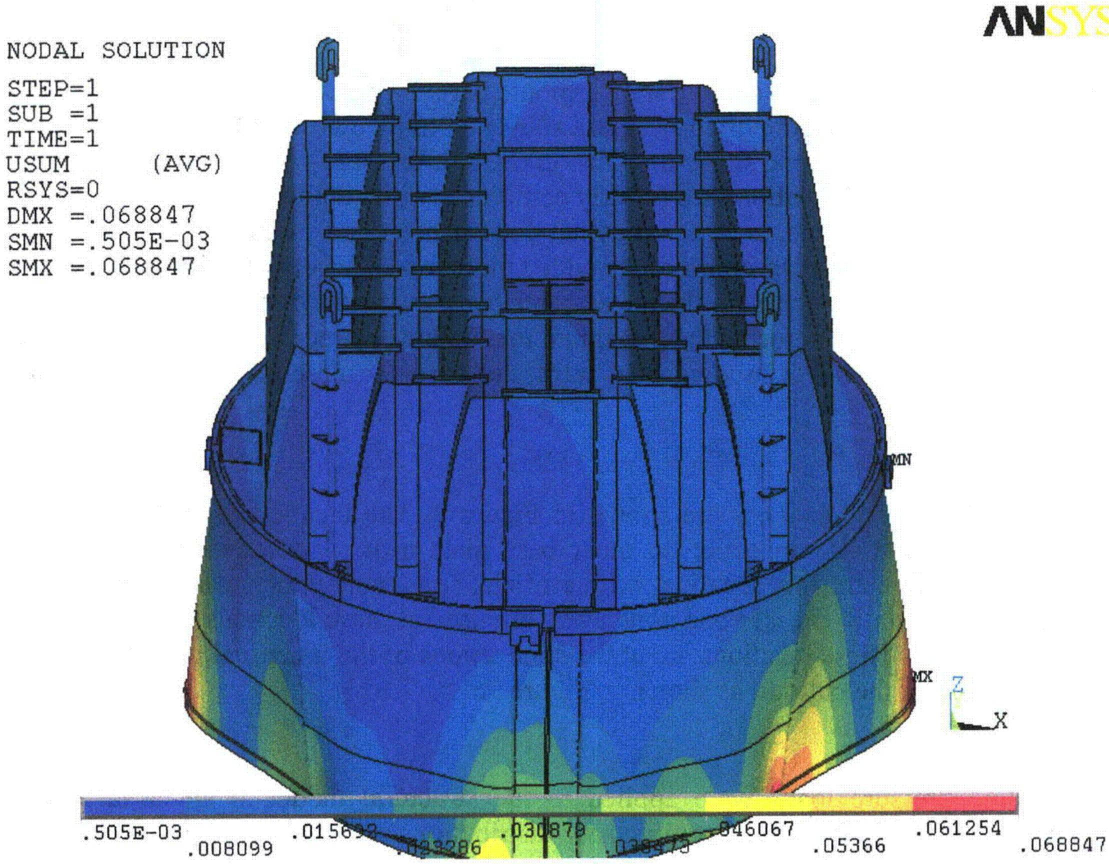

Figure 9a. Overview of static calculations showing displacements (in inches). Maximum displacement (DMX) is 0.069". Note that displacements are amplified for visualization.

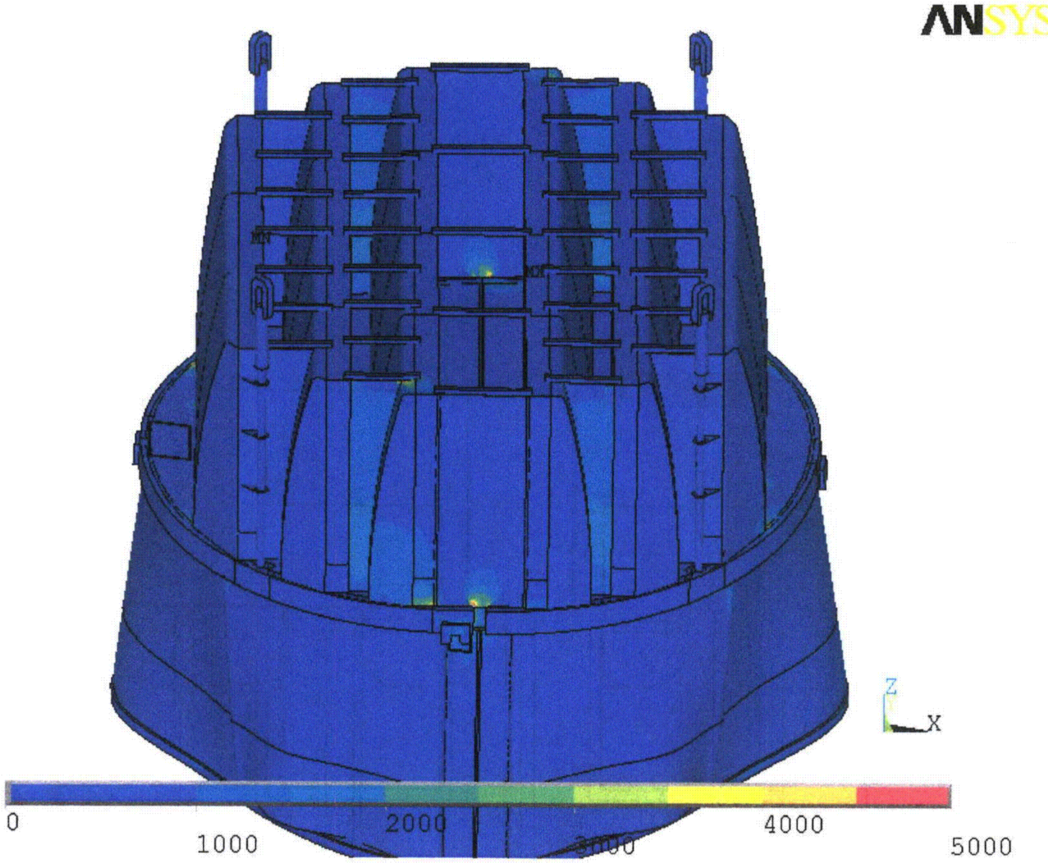

Figure 9b. Overview of static calculations showing stress intensities (in psi). Maximum stress intensity (SMX) is 9,598 psi. Note that displacements are amplified for visualization

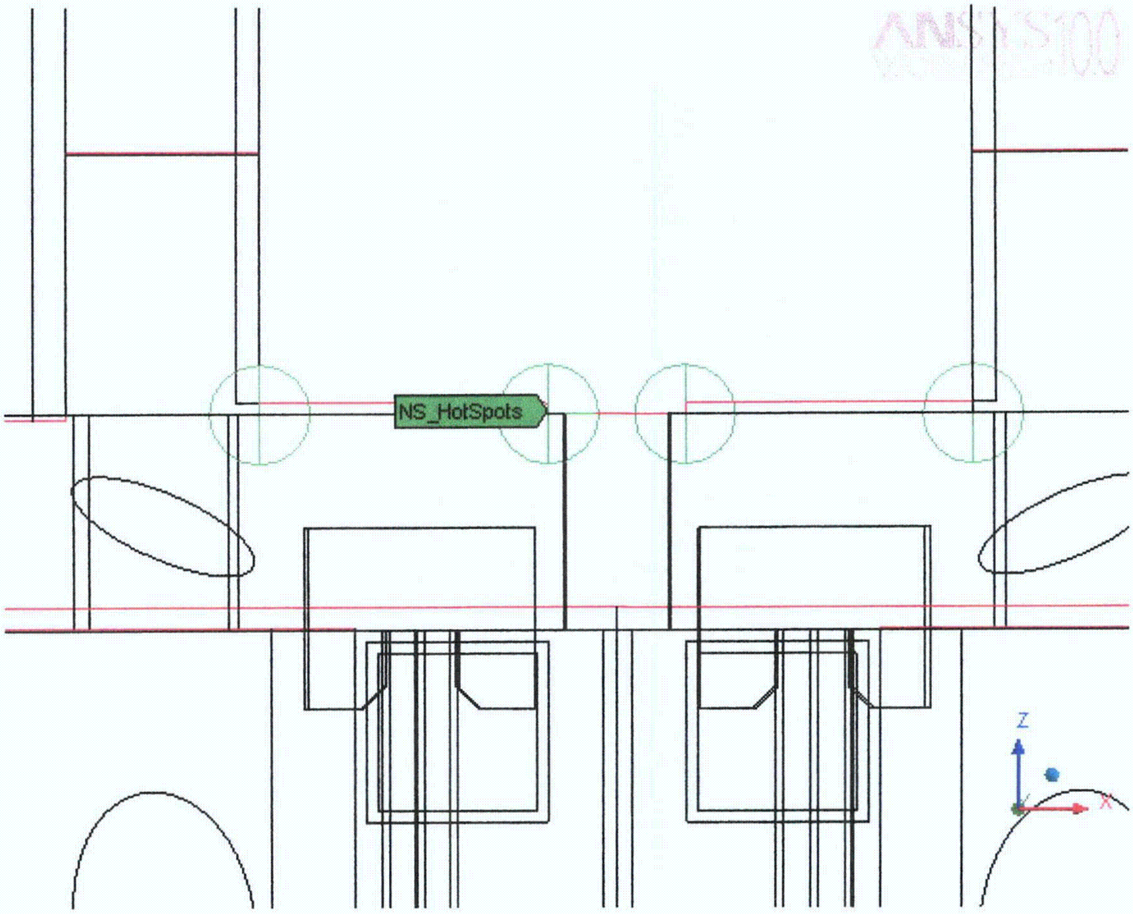

Figure 9c. Stress singularities. Model is shown in wireframe mode for clarity.

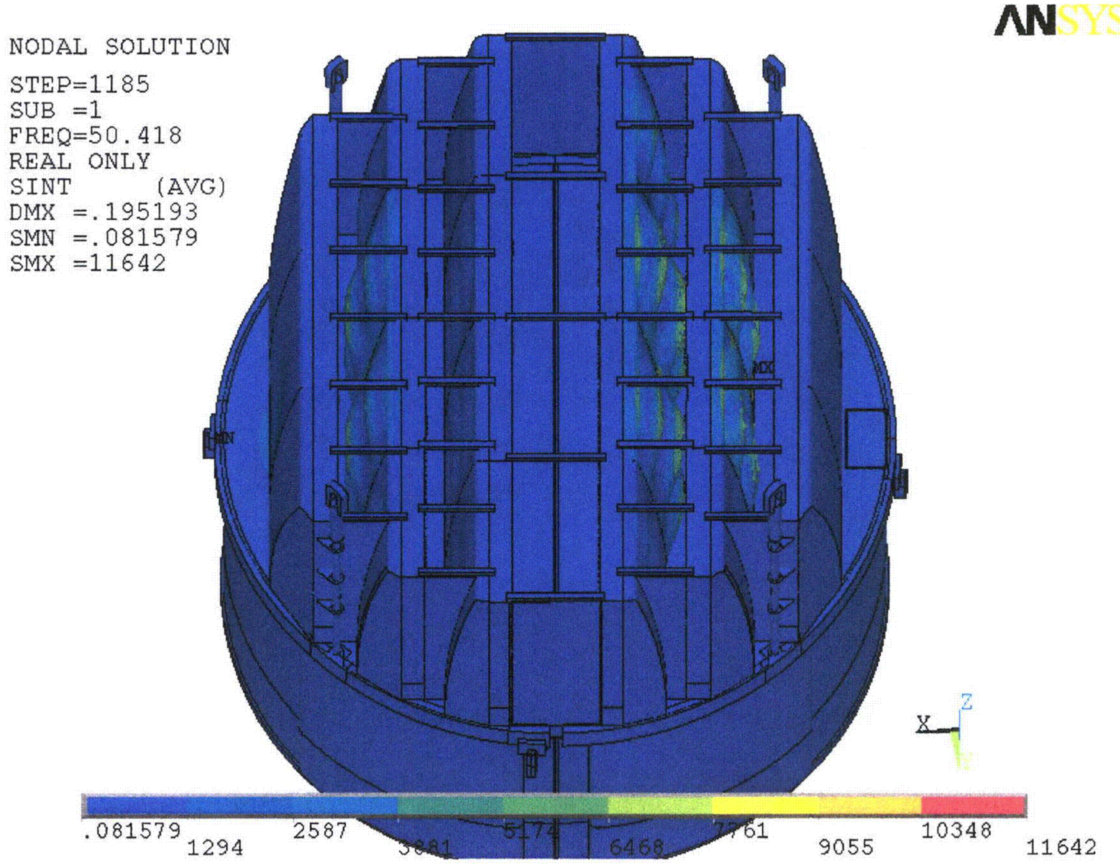

Figure 10a. Overview of harmonic calculations showing real part of stress intensities (in psi) along with displacements. Unit loading MSL A at 50.1 Hz (oriented to show high stress locations at the hoods).

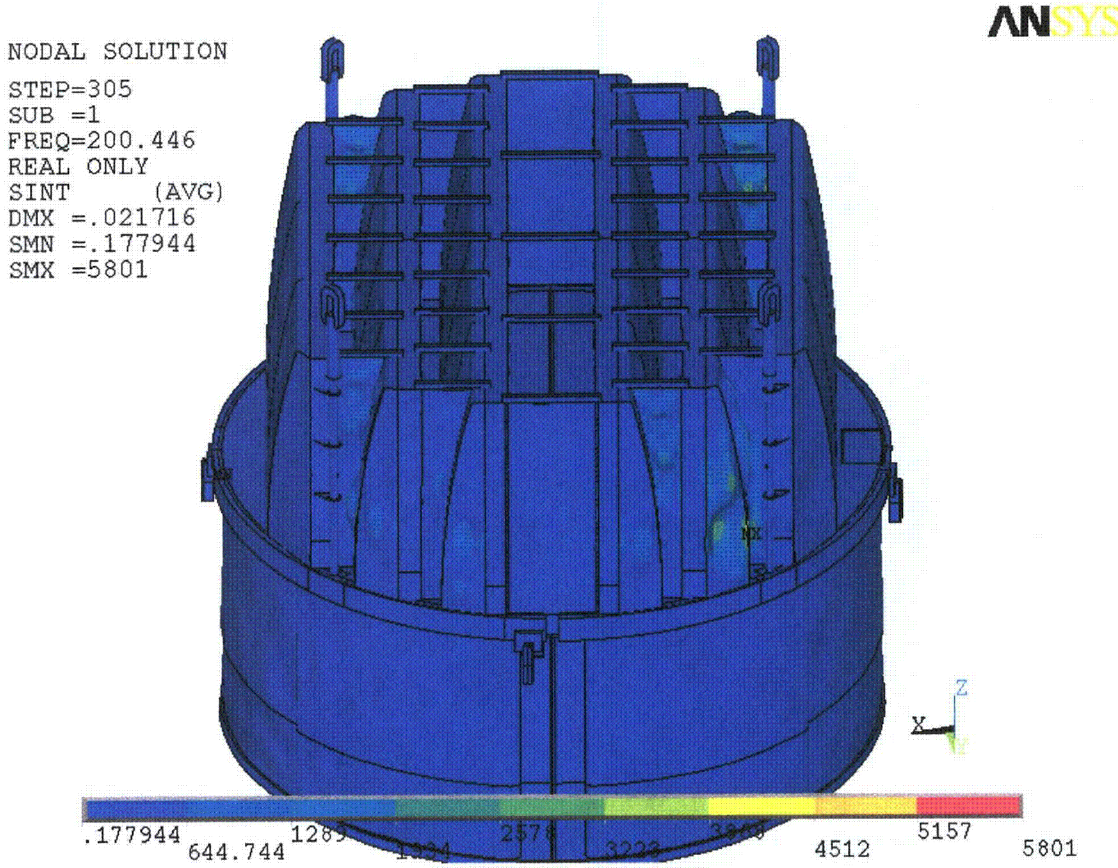

Figure 10b. Overview of harmonic calculations showing real part of stress intensities (in psi) along with displacements. Unit loading MSL A at 200.5 Hz.

4.3 Post-Processing

The static and transient stresses computed at every node with ANSYS were exported into files for subsequent post-processing. These files were then read into separate customized software to compute the maximum and alternating stresses at every node. The maximum stress was defined for each node as the largest stress intensity occurring during the time history. Alternating stresses were calculated according to the ASME standard described above. For shell elements the maximum stresses were calculated separately at the mid-plane, where only membrane stress is present, and at top/bottom of the shell, where bending stresses are also present.

For nodes that are shared between several structural components or lie on junctions, the maximum and alternating stress intensities are calculated as follows. First, the nodal stress tensor is computed separately for each individual component by averaging over all finite elements meeting at the node and belonging to the same structural component. The time histories of these stress tensors are then processed to deduce the maximum and alternating stress intensities for each structural component. Finally for nodes shared across multiple components the highest of the component-wise maximum and alternating stresses is recorded as the "nodal" stress. This approach prevents averaging of stresses across components and thus yields conservative estimates for nodal stresses at the weld locations where several components are joined together.

The maximum stresses are compared against allowable values which depend upon the stress type (membrane, membrane+bending, alternating – Pm, Pm+Pb, S_{alt}) and location (at a weld or away from welds). These allowables are specified in the following section. For solid elements the most conservative allowable for membrane stress, Pm, is used, although bending stresses are nearly always present also. The structure is then assessed in terms of stress ratios formed by dividing allowables by the computed stresses at every node. Stress ratios less than unity imply that the associated maximum and/or alternating stress intensities exceed the allowable levels. Post-processing tools calculate the stress ratios, identifying the nodes with low stress ratios and generating files formatted for input to the 3D graphics program, TecPlot, which provides more general and sophisticated plotting options than currently available in ANSYS.

4.4 Computation of Stress Ratios for Structural Assessment

The ASME B&PV Code, Section III, subsection NG provides different allowable stresses for different load combinations and plant conditions. The stress levels of interest in this analysis are for the normal operating condition, which is the Level A service condition. The load combination for this condition is:

Normal Operating Load Combination = Weight + Pressure + Thermal

The weight and fluctuating pressure contributions have been calculated in this analysis and are included in the stress results. The static pressure differences and thermal expansion stresses are small, since the entire steam dryer is suspended inside the reactor vessel and all surfaces are exposed to the same conditions. Seismic loads only occur in Level B and C cases, and are not considered in this analysis.

Allowable Stress Intensities

The ASME B&PV Code, Section III, subsection NG shows the following (Table 5) for the maximum allowable stress intensity (Sm) and alternating stress intensity (Sa) for the Level A service condition. The allowable stress intensity values for type 304 stainless steel at operating temperature 550°F are taken from Table I-1.2 and Fig. I-9.2.2 of Appendix I of Section III, in the ASME B&PV Code. The calculation for different stress categories is performed in accordance with Fig. NG-3221-1 of Division I, Section III, subsection NG.

Table 5. Maximum Allowable Stress Intensity and Alternating Stress Intensity for all areas other than welds. The notation Pm represents membrane stress; Pb represents stress due to bending; Q represents secondary stresses (from thermal effects and gross structural discontinuities, for example); and F represents additional stress increments (due to local structural discontinuities, for example).

Type	Notation	Service Limit	Allowable Value (ksi)
Maximum Stress Allowables:			
General Membrane	Pm	Sm	16.9
Membrane + Bending	Pm + Pb	1.5 Sm	25.35
Primary + Secondary	Pm + Pb + Q	3.0 Sm	50.7
Alternating Stress Allowable:			
Peak = Primary + Secondary + F	S_{alt}	Sa	13.6

When evaluating welds, either the calculated or allowable stress was adjusted, to account for stress concentration factor and weld quality. Specifically:

- For maximum allowable stress intensity, the allowable value is decreased by multiplying its value in Table 5 by 0.55.
- For alternating stress intensity, the calculated weld stress intensity is multiplied by a weld stress intensity (fatigue) factor of 1.8, before comparison to the Sa value given above.

The weld factors of 0.55 and 1.8 were selected based on the observable quality of the shop welds and liquid penetrant NDE testing of all welds (excluding tack and intermittent welds, which were subject to 5X visual inspection) during fabrication. These factors are consistent with fatigue strength reduction factors recommended by the Welding Research Council, [19], and stress concentration factors at welds, provided in [20] and [21]. In addition, critical welds are subject to periodical visual inspections in accordance with the requirements of GE SIL 644 SIL and BWR VIP-139 [22]. Therefore, for weld stress intensities, the allowable values are shown in Table 6.

These factors (0.55 and 1.8) also conservatively presume that the structure is joined using fillet welds unless specified otherwise. Since fillet welds correspond to larger stress concentration factors than other types of welds, this assumption is a conservative one.

Table 6. Weld Stress Intensities.

Type	Notation	Service Limit	Allowable Value (ksi)
Maximum Stress Allowables:			
General Membrane	Pm	0.55 Sm	9.30
Membrane + Bending	Pm + Pb	0.825 Sm	13.94
Primary + Secondary	Pm + Pb + Q	1.65 Sm	27.89
Alternating Stress Allowables:			
Peak = Primary + Secondary + F	S_{alt}	Sa	13.6

Comparison of Calculated and Allowable Stress Intensities

The classification of stresses into general membrane or membrane + bending types was made according to the exact location, where the stress intensity was calculated; namely, general membrane, Pm, for middle surface of shell element, and membrane + bending, Pm + Pb, for other locations. For solid elements the most conservative, general membrane, Pm, allowable is used.

The structural assessment is carried out by computing stress ratios between the computed maximum and alternating stress intensities, and the allowable levels. Locations where any of the stresses exceed allowable levels will have stress ratios less than unity. Since computation of stress ratios and related quantities within ANSYS is time-consuming and awkward, a separate FORTRAN code was developed to compute the necessary maximum and alternating stress intensities, Pm, Pm+Pb, and S_{alt}, and then compare it to allowables. Specifically, the following quantities were computed at every node:

1. The maximum membrane stress intensity, Pm (evaluated at the mid-thickness location for shells),
2. The maximum membrane+bending stress intensity, Pm+Pb, (taken as the largest of the maximum stress intensity values at the bottom, top, and mid thickness locations, for shells),
3. The alternating stress, S_{alt}, (the maximum value over the three thickness locations is taken).
4. The stress ratio due to a maximum stress intensity assuming the node lies at a non-weld location (note that this is the minimum ratio obtained considering both membrane stresses and membrane+bending stresses):
   SR-P(nw) = min{ Sm/Pm, 1.5 * Sm/(Pm+Pb) }.
5. The alternating stress ratio assuming the node lies at a non-weld location,
   SR-a(nw) = Sa / (1.1 * S_{alt}),
6. The same as 4, but assuming the node lies on a weld,
   SR-P(w)=SR-P(nw) * 0.55
7. The same as 5, but assuming the node lies on a weld,
   SR-a(w)=SR-a(nw) / 1.8.

Note that in steps 4 and 6, the minimum of the stress ratios based on Pm and Pm+Pb, is taken. The allowables listed in Table 6, Sm=16,900 psi and Sa=13,600 psi. The factors, 0.55 and 1.8, are the weld factors discussed above. The factor of 1.1 accounts for the differences in Young's moduli for the steel used in the steam dryer and the values assumed in alternating stress allowable. According to NG-3222.4 in subsection NG of Section III of the ASME Code [2], the effect of elastic modulus upon alternating stresses is taken into account by multiplying alternating stress S_{alt} at all locations by the ratio, $E/E_{model}=1.1$, where:

$E = 28.3\ 10^6$ psi, as shown on Fig. I-9.2.2. ASME BP&V Code
$E_{model} = 25.55\ 10^6$ psi (Table 1)

The appropriate maximum and alternating stress ratios, SR-P and SR-a, are thus determined and a final listing of nodes having the smallest stress ratios is generated. The nodes with stress ratios lower than 4 are plotted in TecPlot (a 3D graphics plotting program widely used in engineering communities [23]). These nodes are tabulated and depicted in the following Results Section.

Finally, at a limited number of weld locations (specifically the vertical hood reinforcement strip), estimates of the 'nominal' membrane and membrane+bending stresses is taken by finding the maximum stress at all of the surrounding non-weld element nodes. This stress is then multiplied by a weld factor of f=4.0 in accordance with the ASME code (Table NG-3352-1). This is the appropriate weld factor for nominal stresses evaluated near, but off the weld and is to be distinguished from the 1.8 (fillet welds) or 1.4 (full penetration welds) weld factors applied to linearized stresses evaluated *on* the weld. This processing of weld stresses is consistent with prior approaches in industry (e.g., [24], specifically Figure 6-46, pg. 112). (Note that the definition of 'nominal' stress is here understood as the characteristic stress in the plate or shell *without* the localized influence of reinforcements or other discontinuities. This definition is not explicitly given in the ASME code which was originally assembled before finite element modeling methods were routinely used and simplified or textbook calculation methods were normative. However, these simplified calculations generally predicted stresses that are in good agreement with the finite element stresses away from junctions. Using neighboring node off-weld stresses to represent the nominal stresses is thus reasonable for engineering application).

4.5 Finite Element Sub-modeling

In order to meet target stress levels at EPU in the NMP2 steam dryer modifications are needed. These consist of stiffening the closure plates (see Appendix A) and reinforcing welds at two locations: (i) the top 18" of the welds connecting the closure plates to the hoods and vane banks and (ii) the weld between the vane bank side plates and lifting rod support brace. These weld reinforcements are developed using high resolution solid element-based sub-models of these locations. The use of localized sub-models is motivated by the need to maintain computational costs at a feasible level. To this end the global steam dryer model is predominantly comprised of shell elements. These elements are well suited for structures such as the steam dryer consisting of shell-like components and tend to produce conservative estimates of the stresses. In some cases however, such as welded junctions involving multiple components, shell element models can overestimate the nominal stress intensities in the vicinity of the junctions. In such cases a more refined analysis using solid elements to capture the complete 3D stress distribution, is warranted. Therefore, to efficiently analyze complex structures such as steam dryers, a standard engineering practice is to first analyze the structure using a shell-based model. Locations with high stresses are examined in greater detail using 3D solid elements to obtain a more definitive stress prediction.

The solid element-based sub-modeling follows the procedure outlined in Appendix A (also [25] and Appendix A of [26]) and validated in against both high resolution solid models of the full structure and sub-structuring results in [27] and [28]. Based on these models, the nominal stress intensities computed by the 3D solid element model are lower than those obtained with the shell-based FEA used to analyze the complete steam dryer by the stress reduction factors (SRFs) summarized in Table 7. Note that the SRFs vary according to location being dependent on the individual geometry and also the general loading characteristics. They are generally less than unity due to conservative stress estimates in the shell-based weld stresses. For example the discontinuity stresses computed in a shell model at a weld joint between two orthogonal members are often quite conservative because the shell element depiction does not provide any credit for the stress distribution associated with the specific weld geometry. Once the SRFs are obtained, the stress intensities predicted by the global shell element-based analysis at these locations are first multiplied by these SRFs to obtain more accurate estimates of the nominal stresses. These are then multiplied by the 1.8 weld factor before comparing against allowable stress limits to obtain the alternating stress ratios.

Detailed 3D solid element sub-models are applied at both the weld reinforcements and additional locations (see Table 7 for a complete list). For the closure plate the welds connecting the closure plate to the vane banks and hoods experience significant vibratory stresses due to a plate response in the 125-135 Hz frequency range. Though stresses remain well above allowable levels for all frequency shifts at both CLTP and EPU, the margin is below the target level (i.e., a stress ratio of SR-a=2.0 at EPU). Therefore, the closure plate was reinforced and a sub-model developed for each of the locations on the closure plates where stresses exceeded target levels. On each closure plate there are four such locations. The first two are on the vertical weld joining the closure plate to the vane bank. The first node is at the top of this weld and the second one lies 13.5" below it. The other two locations are on the curved weld connecting the closure plate to the curved hood. Again the first location is at the top of this weld and the second one lies 14.5" below it. In both cases, the stresses at the top location result from a combination of membrane and bending stresses whereas the stresses at the lower locations are predominantly due to bending. The stresses are induced by a closure plate response dominated by a (1,2) mode (i.e., the mode shape resembles the first mode of a beam in the horizontal direction and the second mode in the vertical sense) which explains the high stress at the lower locations on the welds. Sub-model calculations at these locations show that to achieve the required target stress levels, an interior weld must be added along the top 18" of each weld thus effectively converting it from a single-sided to a double-sided fillet weld along this length. Additional details are given in Appendix A.

Sub-modeling is also applied to analyze the stresses in the lifting rod support brace where it connects to the vane bank side plate [29]. A sub-modeling analysis of the high stress location shows that for the current ¼" double-sided fillet weld the stress reduction is minimal. Repeating the sub-model analysis with an increased weld of 1/2" resulted in a stress reduction factor of 0.60. To meet EPU target stress levels it is recommended to increase the weld to this size.

The other locations where sub-modeling was performed are listed as locations 6-9 in Table 7 and involve hood/hood support weld and the bottom of this weld where it meets the base plate junction as well as two locations near tie bar ends involving large welds that are not accounted for in the shell model. The locations of all sub-models are depicted in Figure 11. Additional details of sub-models evaluated for locations away from the closure plate are given in [29].

Table 7. Summary of stress reduction factors obtained using sub-model analysis.

	Location	Stress Reduction Factor
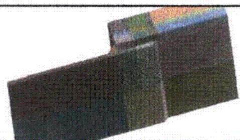	1. Top of vertical closure plate/vane bank weld	0.62 (Appendix A)
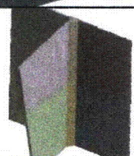	2. 14.5" below location 3 on the same weld	0.71 (Appendix A)
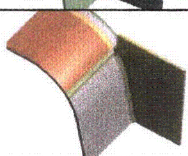	3. Top of closure plate/hood weld	0.86 (Appendix A)
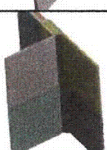	4. 13.5" below location 1 on the same weld	0.88 (Appendix A)
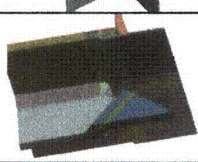	5. Lifting rod support brace/vane side plate junction (assuming an increased 1/2" weld)	0.60 [29]
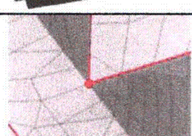	6. Bottom of hood/hood support weld at junction with base plate	0.79 [25]
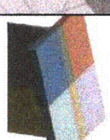	7. Hood/hood support	0.77 [26]
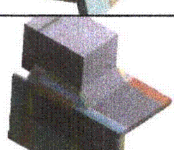	8. Side plate/top plate	0.70 [29]
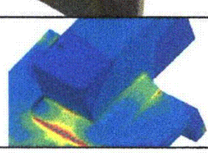	9. Tie bar/top vane bank plate.	0.71 [29]

Note: For locations 1-4 it is assumed that an inner weld has been to the top 18" of the welds joining the closure plate to the hoods or vane banks, thereby replacing the existing single-sided fillet weld by one that is double sided. Also, an increased ½" weld is assumed for location 5.

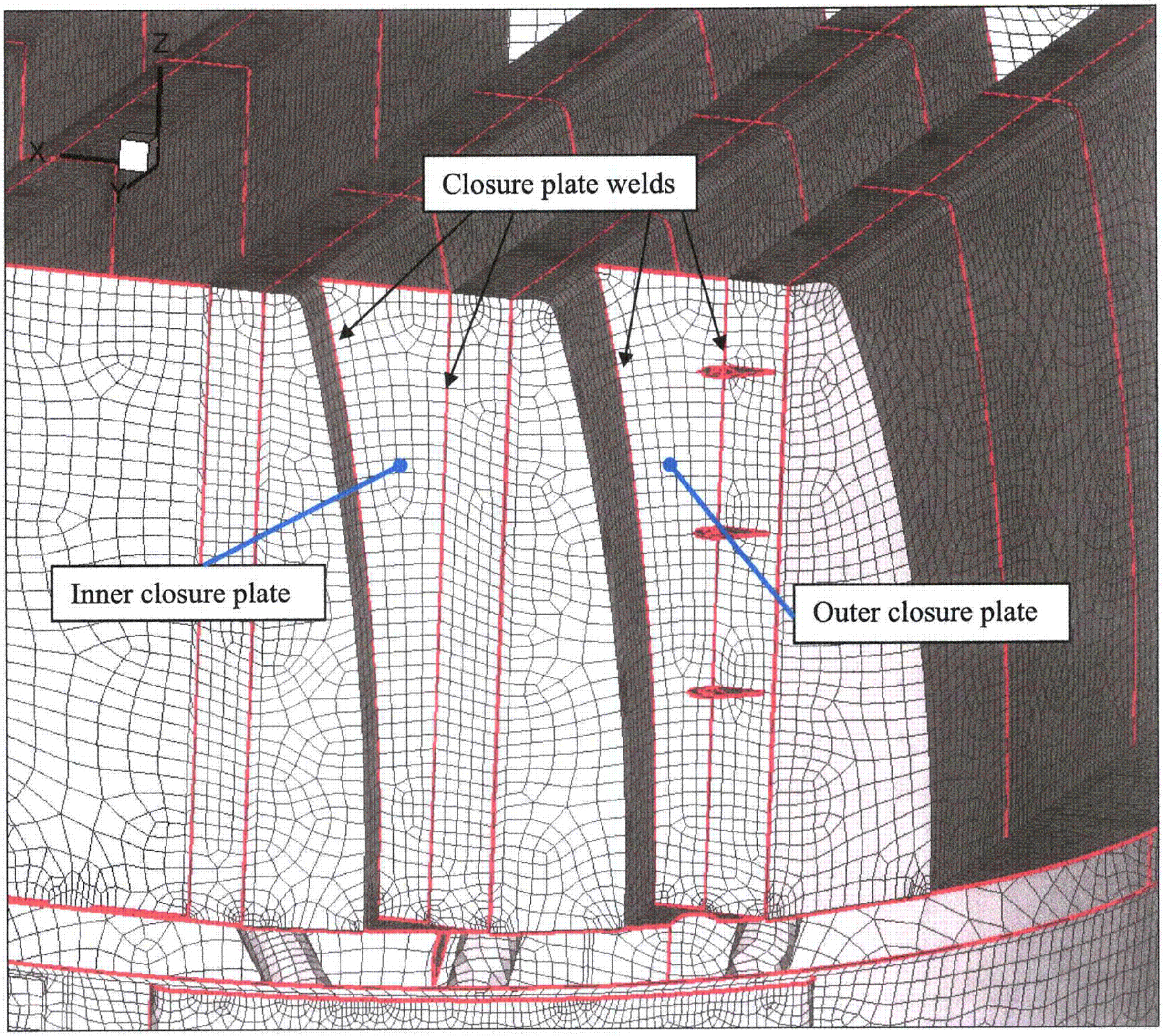

Figure 11a. Closure plates and associated attachment welds examined with sub-model in Appendix A (note lifting rods and other components modeled with solid elements are omitted for clarity). Sub-models on the perimeter are locations 1-4 in Table 7.

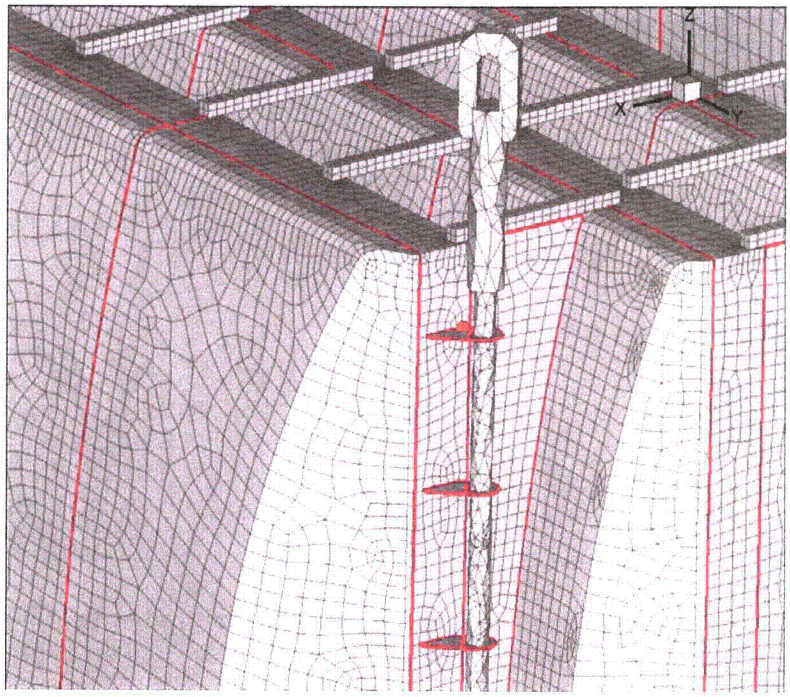

Figure 11b. Location of node on inner hood/hood support/middle base plate weld analyzed with sub-model in [29]. Sub-model corresponds to location 5 in Table 7.

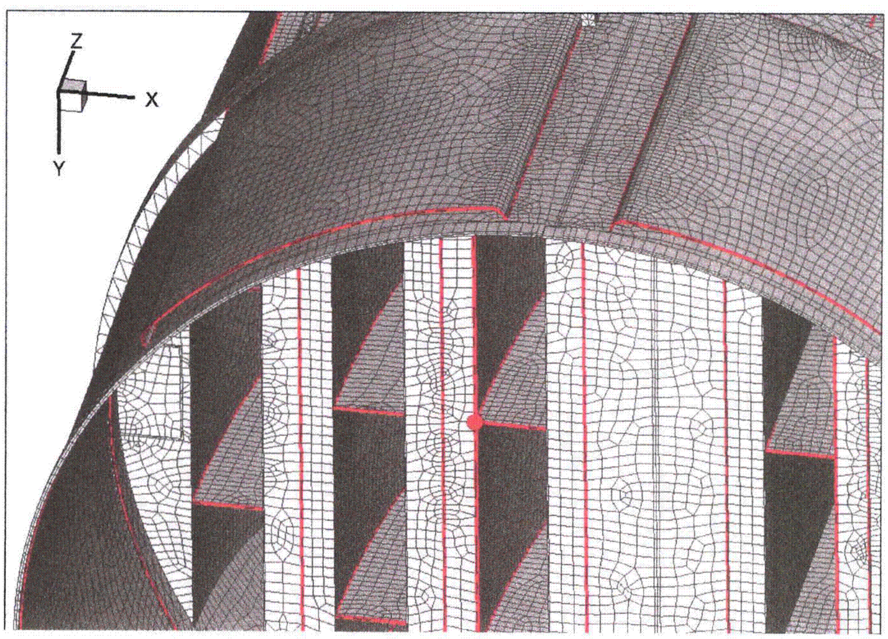

Figure 11c. Location of node on hood/hood support/base plate weld analyzed with sub-model in [25]. Sub-model corresponds to location 6 in Table 7.

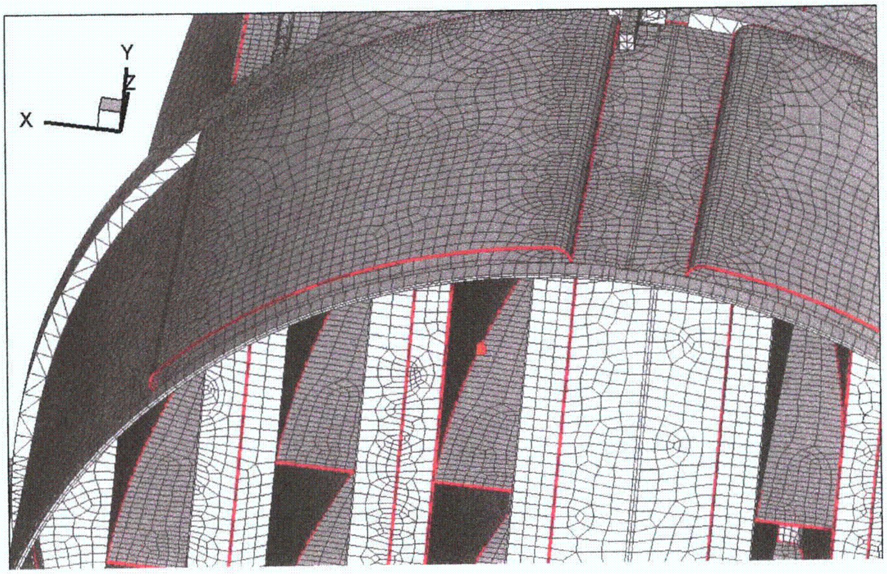

Figure 11d. Location of node on hood/hood support weld analyzed with sub-model analysis procedure in [26]. Sub-model corresponds to location 7 in Table 7.

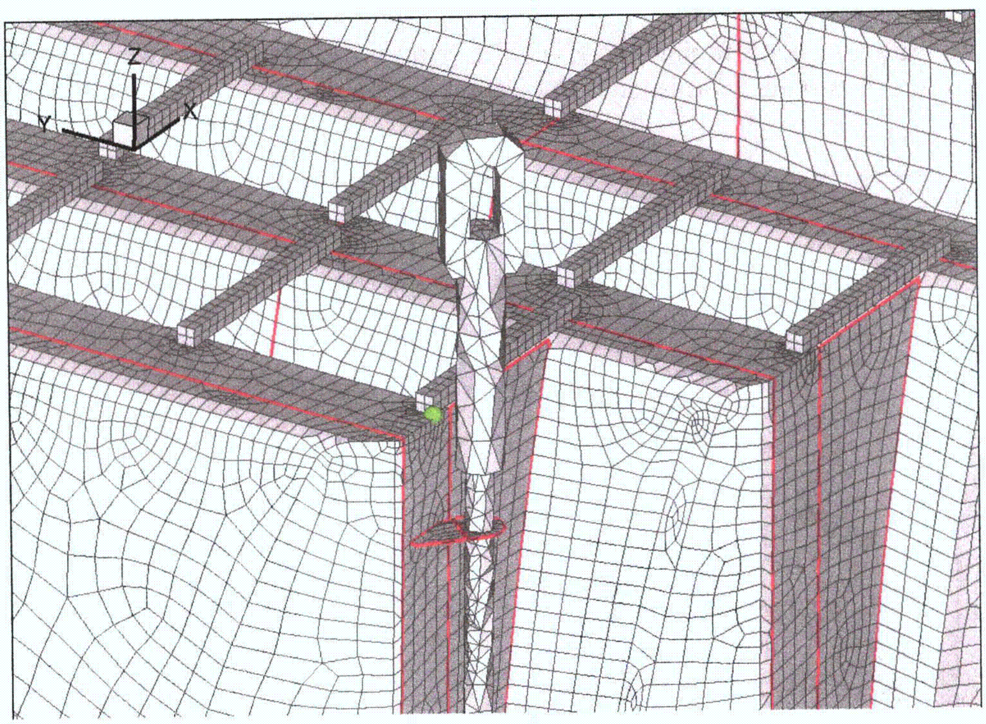

Figure 11e. Location of node on side plate/top plate weld analyzed with sub-model analysis procedure in [29]. Sub-model corresponds to location 8 in Table 7.

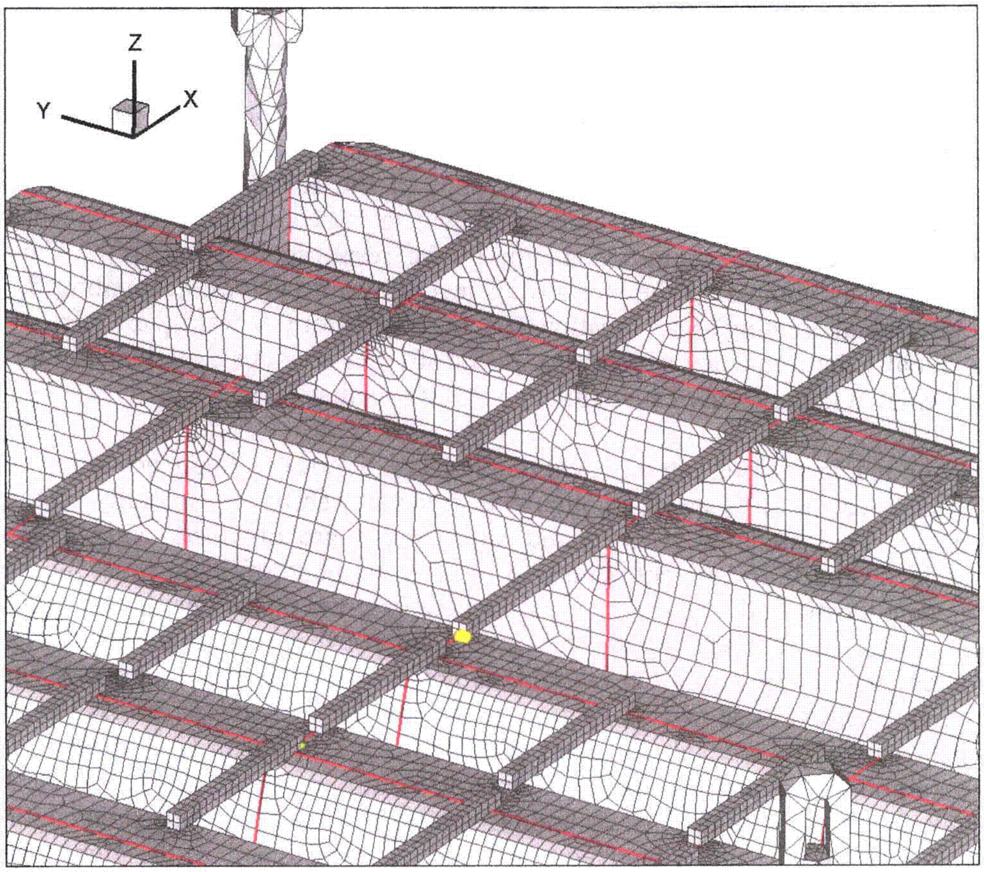

Figure 11f. Location of node on tie bar/top vane bank plate weld analyzed with sub-model analysis procedure in [29]. Sub-model corresponds to location 9 in Table 7.

5. Results

The stress intensities and associated stress ratios resulting from the Rev. 4 acoustic/hydrodynamic loads [4] with associated biases and uncertainties factored in, are presented below. The bias due to finite frequency discretization and uncertainty associated with the finite element model itself, are also factored in. In the following sections the highest maximum and alternating stress intensities are presented to indicate which points on the dryer experience significant stress concentration and/or modal response (Section 5.1). The lowest stress ratios obtained by comparing the stresses against allowable values, accounting for stress type (maximum and alternating) and location (on or away from a weld), are also reported (Section 5.2). Finally the frequency dependence of the stresses at nodes experiencing the lowest stress ratios is depicted in the form of accumulative PSDs (Section 5.3).

In each section results are presented both at nominal conditions (no frequency shift) and with frequency shift included. Unless specified otherwise, frequency shifts are generally performed at 2.5% increments. The tabulated stresses and stress ratios are obtained using a 'blanking' procedure that is designed to prevent reporting a large number of high stress nodes from essentially the same location on the structure. In the case of stress intensities this procedure is as follows. The relevant stress intensities are first computed at every node and then nodes sorted according to stress level. The highest stress node is noted and all neighboring nodes within 10 inches of the highest stress node and its symmetric images (i.e., reflections across the x=0 and y=0 planes) are "blanked" (i.e., excluded from the search for subsequent high stress locations). Of the remaining nodes, the next highest stress node is identified and its neighbors (closer than 10 inches) blanked. The third highest stress node is similarly located and the search continued in this fashion until all nodes are either blanked or have stresses less than half the highest value on the structure. For stress ratios, an analogous blanking procedure is applied. Thus the lowest stress ratio of a particular type in a 10" neighborhood and its symmetric images is identified and all other nodes in these regions excluded from listing in the table. Of the remaining nodes, the one with the lowest stress ratio is reported and its neighboring points similarly excluded, and so on until all nodes are either blanked or have a stress ratio higher than 4.

The measured CLTP strain gage signals contain significant contributions from non-acoustic sources such as sensor noise, MSL turbulence and pipe bending vibration that contribute to the hoop strain measurements. The ACM analysis does not distinguish between the acoustic and non-acoustic fluctuations in the MSL signals that could lead to sizeable, but fictitious acoustic loads and resulting stresses on the dryer. One way to filter these fictitious loads is to collect data with the system maintained at operating pressure (1000 psi) and temperature, but low power [30]. By operating the recirculation pumps at this condition, the background plant noise and vibrations remain present. At these conditions the acoustic loads are known to be negligible so that collected data, referred to as the low power data, originate entirely from non-acoustic sources such as sensor noise and mechanical vibrations. This information is valuable since it allows one to now distinguish between the acoustic and non-acoustic content in the CLTP signal and therefore modify the CLTP loads so that only the acoustic component is retained. In previous analyses of the similar dryers, these low power signals were subtracted.

In the present implementation however, no filtering using low power data is performed. The reason for retaining noise in this particular case is to avoid protracted review of the low power subtraction process and to thus expedite qualification of the dryer. Thus, rather than attempting to justify the use of low power noise subtraction in this case, it was decided to use the CLTP signal (and by extension the EPU signals) directly without noise filtering. Therefore for all results presented herein, no noise filtering using low power data has been performed.

The applied load includes all biases and uncertainties for both the ACM (summarized in [4]) and the FEM. For the latter there are three main contributors to the bias and uncertainty. The first is an uncertainty (25.26%) that accounts for modeling idealizations (e.g., vane bank mass model), geometrical approximations and other discrepancies between the modeled and actual dryer such as neglecting of weld mass and stiffness in the FEA. The second contributor is a bias of 9.53% accounting for discretization errors associated with using a finite size mesh, upon computed stresses. The third contributor is also a bias and compensates for the use of a finite discretization schedule in the construction of the unit solutions. The frequencies are spaced such that at 1% damping the maximum (worst case) error in a resonance peak is 5%. The average error for this frequency schedule is 1.72%.

It is significant to note that the applied loads reflect revised bias and uncertainty values over new frequency intervals: 60-70 Hz and 70-100 Hz. The higher bias and uncertainty values in the 60-70 Hz range strongly influence the limiting stresses values, but are also overly conservative. This is because when specifying new frequency intervals the ACM should be recalibrated over these intervals before calculating the bias and uncertainty values. Because it is resource-intensive and would constitute further revisions to the ACM model (to Rev. 5) this model re-calibration was not performed. Consequently the revised biases and uncertainties are higher than they would be if the ACM had been matched to data over the new intervals.

5.1 General Stress Distribution and High Stress Locations

The maximum stress intensities obtained by post-processing the ANSYS stress histories for CLTP at nominal frequency and with frequency shift operating conditions are listed in Table 8. Contour plots of the stress intensities over the steam dryer structure are shown on Figure 12 (nominal frequency) and Figure 13 (maximum stress over all nine frequency shifts including nominal). The figures are oriented to emphasize the high stress regions. Note that these stress intensities *do not* account for weld factors but include end-to-end bias and uncertainty. Further, it should be noted that since the allowable stresses vary with location, stress intensities do not necessarily correspond to regions of primary structural concern. Instead, structural evaluation is more accurately made in terms of the stress ratios which compare the computed stresses to allowable levels with due account made for stress type and weld. Comparisons on the basis of stress ratios are made in Section 5.2.

The maximum stress intensities in most areas are low (less than 500 psi). For the membrane stresses (Pm) the high stress regions tend to occur at: (i) the bottom of the central vertical side plate that joins the innermost vane banks (stress concentrations occur where this plate is welded to the inner base plates resting on the upper support ring); (ii) the welds joining the tie bars to the top cover plates on the vane banks; (iii) the seismic blocks that rest on the steam dryer supports; and (iv) junctions connecting the bottoms of the hood supports. Except for the last location, the stresses are dominated by the static contribution as can be inferred from the small alternating stress intensities (Salt) tabulated in Table 8 for the high Pm locations. From Figure 12a and Figure 13a higher Pm regions are seen to be in the vicinity of the supports where all of the dryer deadweight is transmitted, the closure plates connecting the inner hoods to the middle vane banks, and various localized concentrations such those along the bottom of the outer hood.

The membrane + bending stress (Pm+Pb) distributions evidence a more pronounced modal response especially on the hood structures. The two locations with the highest stress intensities of this type are the same pair having the highest membrane stress and are dominated by deadweight. High stress concentration is also recorded on the top edge of this vertical plate where it joins to the inner vane bank. Other areas with high Pm+Pb stress concentrations include: (i) the tops of the closure plates where they are welded to a hood or vane bank end plates; (ii) the skirt/drain channel welds; (iii) the outer cover plates connecting to the upper support ring and bottom of the outer hoods; and (iv) the common junction between each hood, its hood support (or stiffener), and the adjoining base plate (see Figure 13c).

The alternating stress, S_{alt}, distributions are most pronounced on the outer hoods directly exposed to the MSL inlet acoustics, and on welds involving the closure plates. All hoods exhibit a strong response (e.g., Figure 13d). The highest stress intensity at any frequency shift occurs at the middle hood. Though not exposed directly to the MSL acoustic sources, the interior hoods are thinner and their response is driven mainly by structural coupling rather than direct forcing. Numerous weld locations also show significant stress including the bottoms of drain channels and the junctions between the hoods, hood supports and base plates. These locations are characterized by localized stress concentrations as indicated in Figure 13e and have emerged as high stress locations in other steam-dryers also. Other locations with high alternating stress intensities include the tie bar/top cover plate weld and welds involving the closure plate.

Comparing the nominal results (Table 8a) and results with frequency shifting it can be seen that maximum stress intensities, Pm and Pm+Pb, do not differ significantly. The highest alternating stress is approximately 4.2% higher when frequency shifts are considered. For other nodes however the variations are higher. As shown in the next section, all stresses are well within allowable levels.

Table 8a. Locations with highest predicted stress intensities for CLTP conditions with no frequency shift.

Stress Category	Location	Weld	Location (in)			node(a)	Stress Intensities (psi)		
			x	y	z		Pm	Pm+Pb	S_{alt}
Pm	Inner Side Plate	No	3.1	119	0.5	37229	7475	8836	460
"	Side Plate Ext/Inner Base Plate	Yes	16.3	119	0	94143	6913	9809	438
"	Upper Support Ring/Support/Seismic Block	Yes	-6.9	-122.3	-9.5	113554	6238	6238	911
"	Tie Bar	Yes	49.3	108.1	88	141275	5962	5962	807
"	Hood Support/Middle Base Plate/Inner Backing Bar/Inner Hood	Yes	39.9	-59.5	0	101435	5352	5488	1638
Pm+Pb	Side Plate Ext/Inner Base Plate	Yes	16.3	119	0	94143	6913	9809	438
"	Inner Side Plate	No	3.1	119	0.5	37229	7475	8836	460
"	Side Plate/Top Plate	Yes	49.6	108.6	88	93256	2505	8542	1129
"	Middle Base Plate/Inner Backing Bar Out/Inner Backing Bar/Inner Hood	Yes	-39.9	-108.6	0	84197	441	7227	1433
"	Side Plate/Top Plate	Yes	17.6	119	88	91215	898	7174	1337
S_{alt}	Middle Hood	No	-68.9	69.6	41.6	31054	1717	2759	2728
"	Hood Support/Inner Hood	Yes	36.2	0	50.8	99529	975	2316	2290
"	Outer Hood	No	-97.3	-50.7	62	78572	770	2160	2116
"	Middle Hood	No	-67.1	70.9	54.5	31441	1517	2099	2016
"	Hood Support/Inner Hood	Yes	39.1	0	23	99515	842	2064	1977

Notes.
(a) Node numbers are retained for further reference.
(1-9) Appropriate stress reduction factor for the welds and modifications listed in Table 7 have been applied. The number refers to the particular location and corresponding stress reduction factor in Table 7.

Table 8b. Locations with highest predicted stress intensities taken over all frequency shifts CLTP conditions.

Stress Category	Location	Weld	Location (in)			node(a)	Stress Intensities (psi)			% Freq. Shift
			x	y	z		Pm	Pm+Pb	S_{alt}	
Pm	Inner Side Plate	No	3.1	119	0.5	37229	7490	9003	634	10
"	Side Plate Ext/Inner Base Plate	Yes	16.3	119	0	94143	6918	9809	478	5
"	Upper Support Ring/Support/Seismic Block	Yes	-6.9	-122.3	-9.5	113554	6688	6688	1342	5
"	Tie Bar	Yes	-49.3	-108.1	88	143795	6077	6077	877	5
"	Hood Support/Middle Base Plate/Inner Backing Bar/Inner Hood	Yes	39.9	-59.5	0	85723	5495	5819	1815	-10
Pm+Pb	Side Plate Ext/Inner Base Plate	Yes	16.3	119	0	94143	6918	9809	478	0
"	Inner Side Plate	No	3.1	119	0.5	37229	7490	9003	634	5
"	Side Plate/Top Plate	Yes	49.6	108.6	88	93256	2526	8571	1215	5
"	Middle Base Plate/Inner Backing Bar Out/Inner Backing Bar/Inner Hood	Yes	-39.9	-108.6	0	84197	470	7712	1683	5
"	Side Plate/Top Plate	Yes	17.6	119	88	91215	920	7332	1585	5
S_{alt}	Middle hood	No	-68.6	69.6	43.7	31149	1717	2953	2914	2.5
"	Outer hood	No	-97.3	-50.7	62	78572	969	2674	2622	5
"	Closure plate	No	46.2	-108.6	88	16192	3697	5410	2561	10
"	Hood Support/Middle Base Plate/Inner Backing Bar/Inner Hood(6)	Yes	-39.9	0	0	85723	4695	4849	2378	-5
"	Closure plate	No	-70.8	85.2	71.9	17691	271	2394	2355	-10

Notes.
(a) Node numbers are retained for further reference.
(1-9) Appropriate stress reduction factor for the welds and modifications listed in Table 7 have been applied. The number refers to the particular location and corresponding stress reduction factor in Table 7.

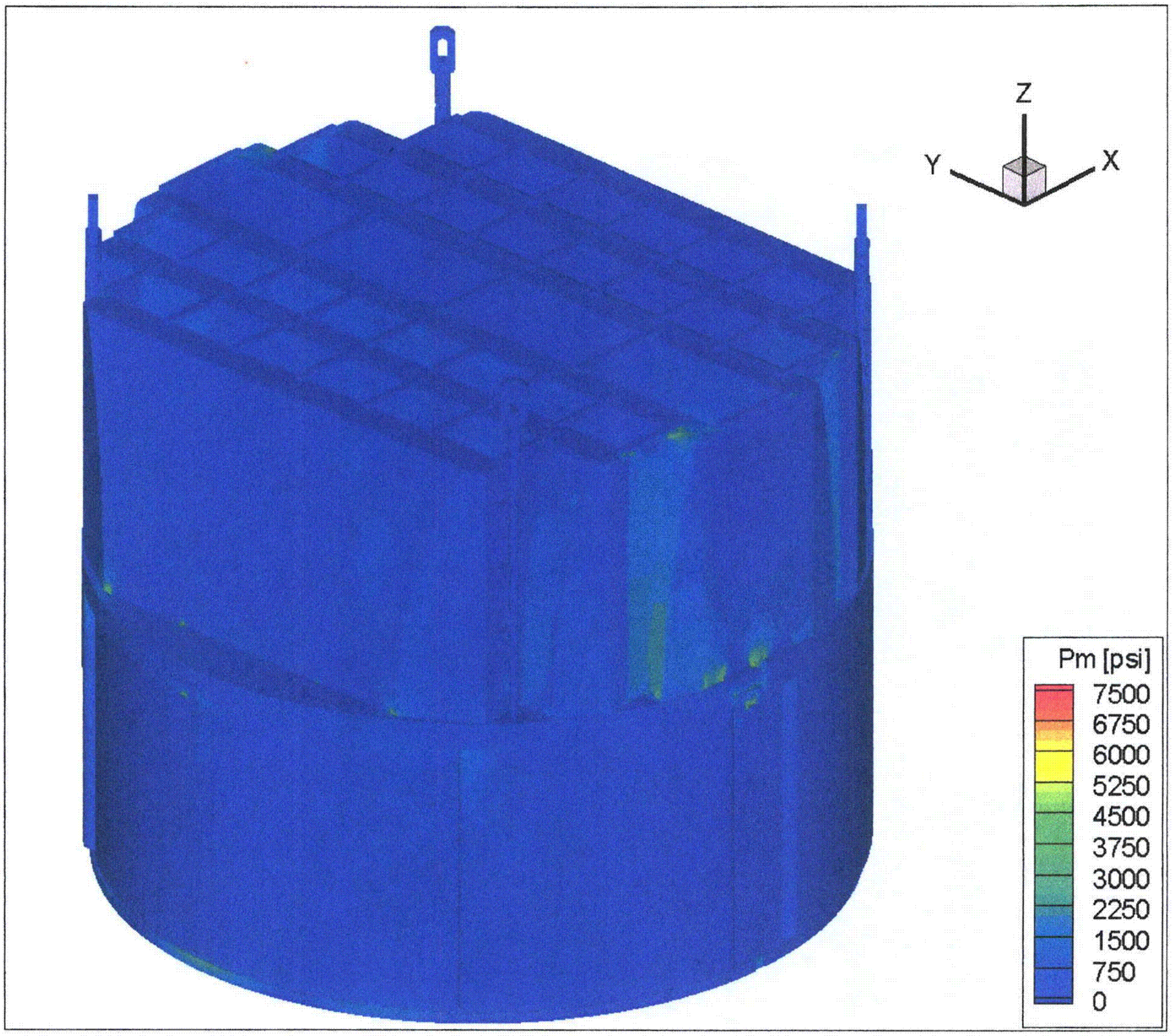

Figure 12a. Contour plot of maximum membrane stress intensity, Pm, for CLTP load. The maximum stress intensity is 7475 psi.

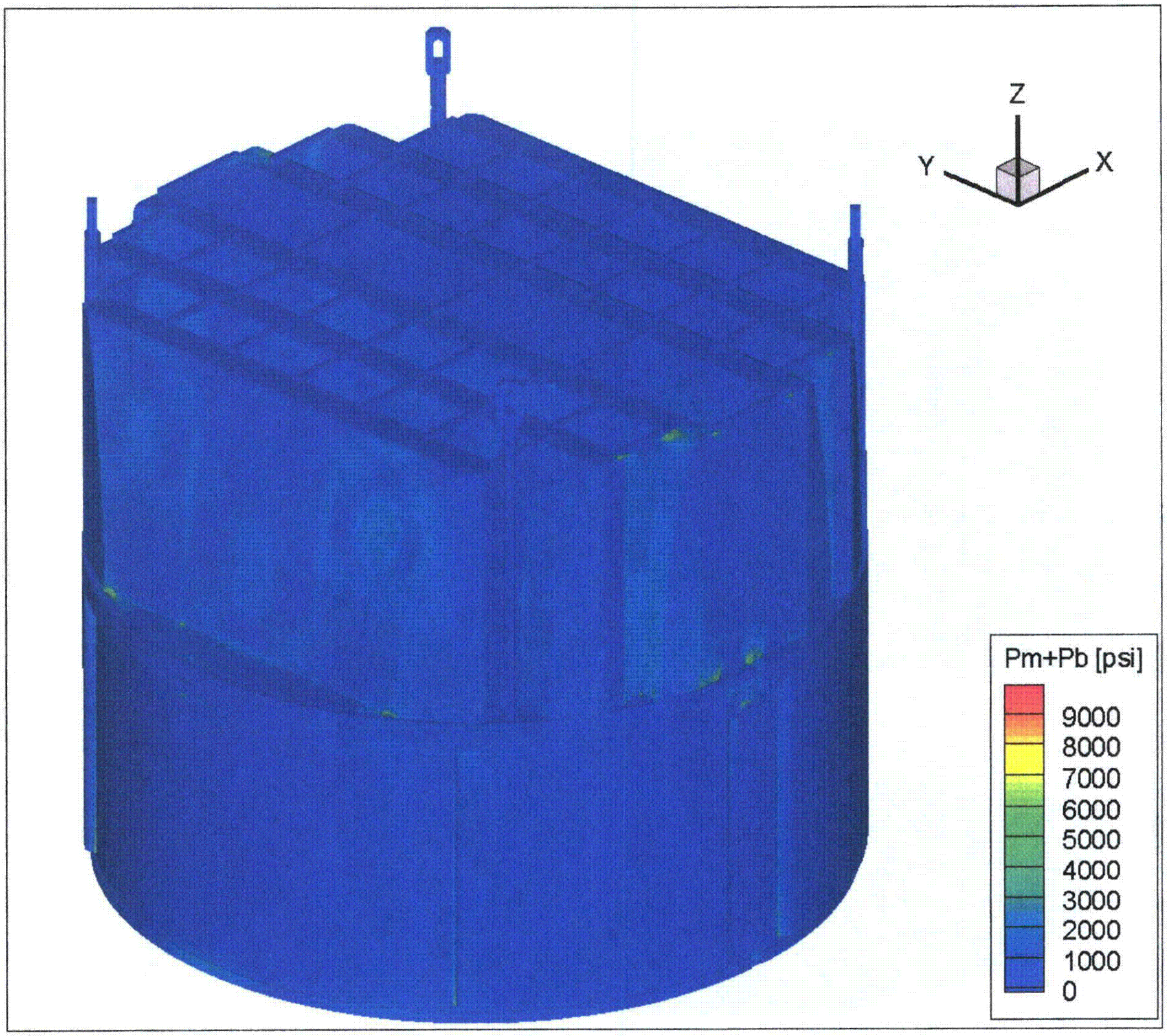

Figure 12b. Contour plot of maximum membrane+bending stress intensity, Pm+Pb, for CLTP load. The maximum stress intensity is 9809 psi. First view.

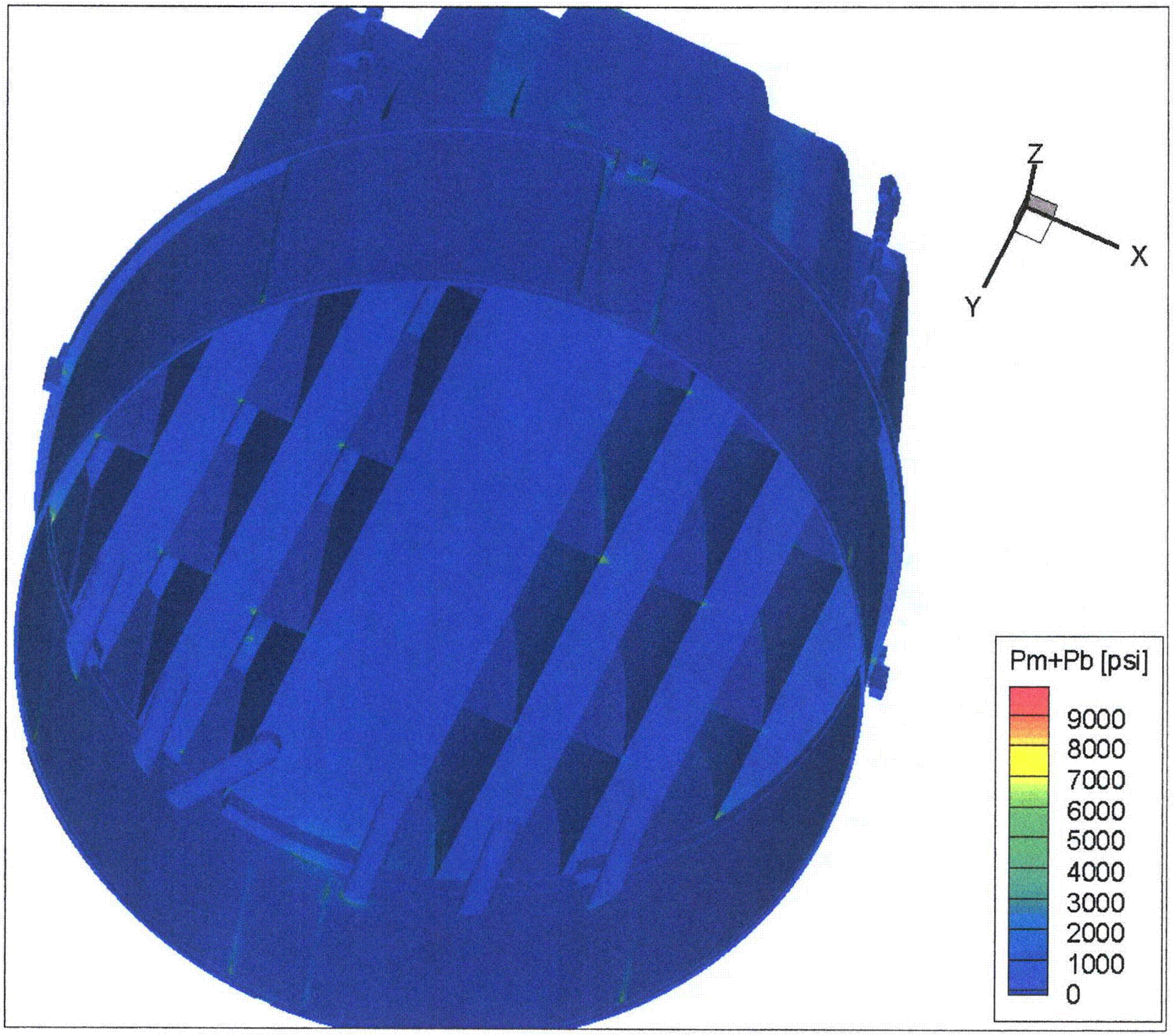

Figure 12c. Contour plot of maximum membrane+bending stress intensity, Pm+Pb, for CLTP load. This second view from below shows the high stress intensities at the hood/stiffener/base plate junctions and drain channel/skirt welds.

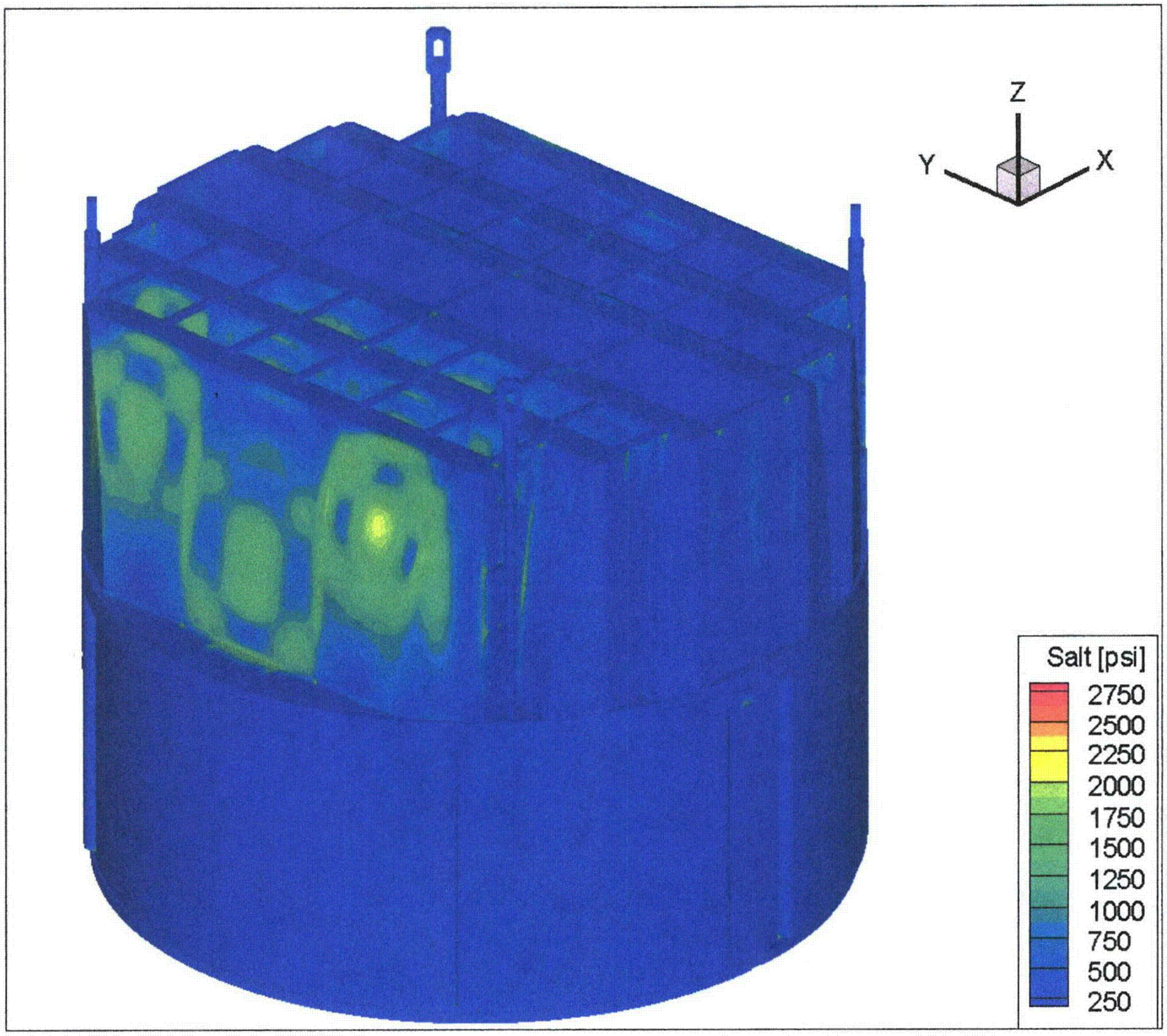

Figure 12d. Contour plot of alternating stress intensity, S_{alt}, for CLTP load. The maximum alternating stress intensity is 2728 psi. First view.

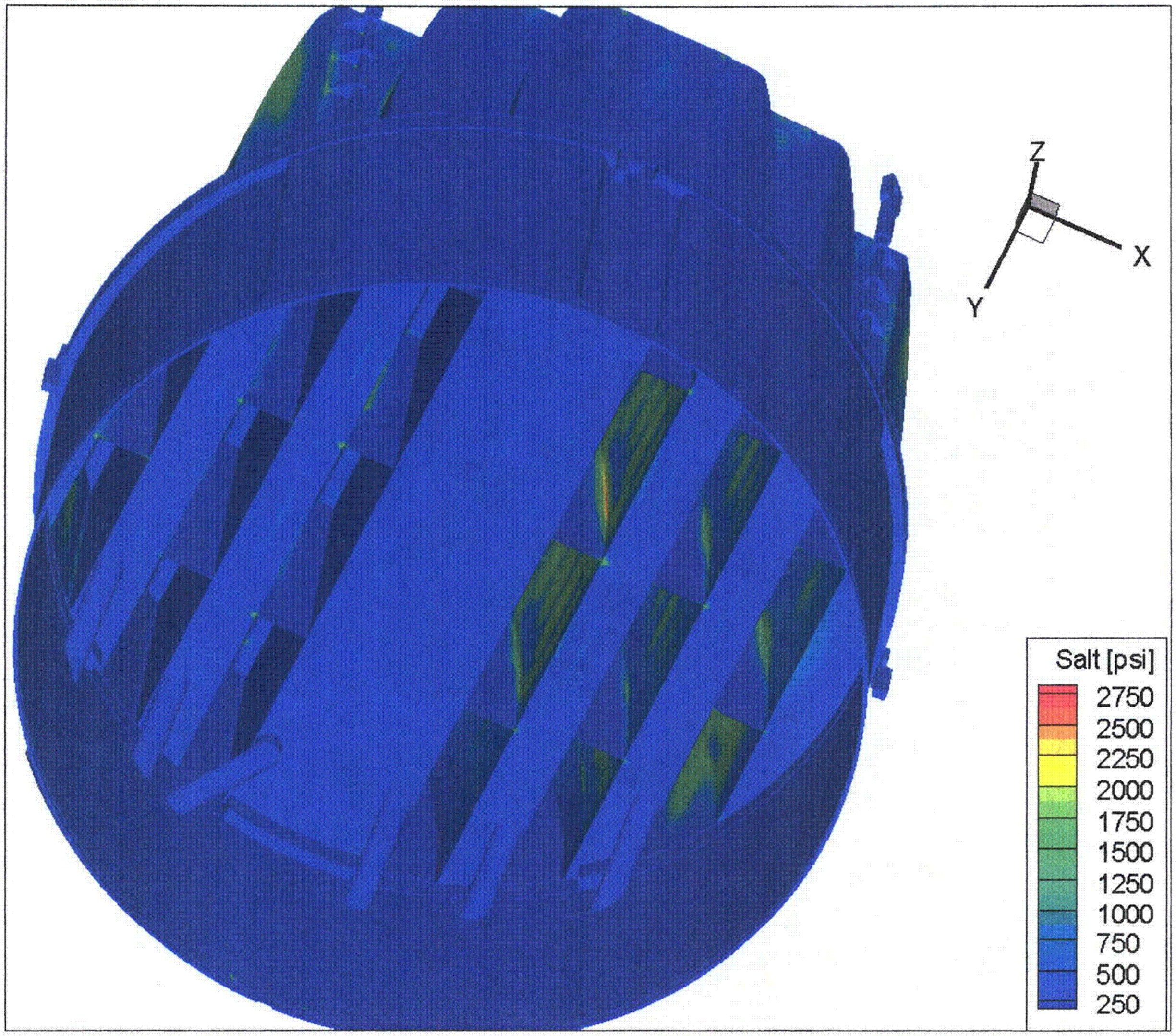

Figure 12e. Contour plot of alternating stress intensity, S_{alt}, for CLTP load. Second view showing details of the outer hood and closure plate.

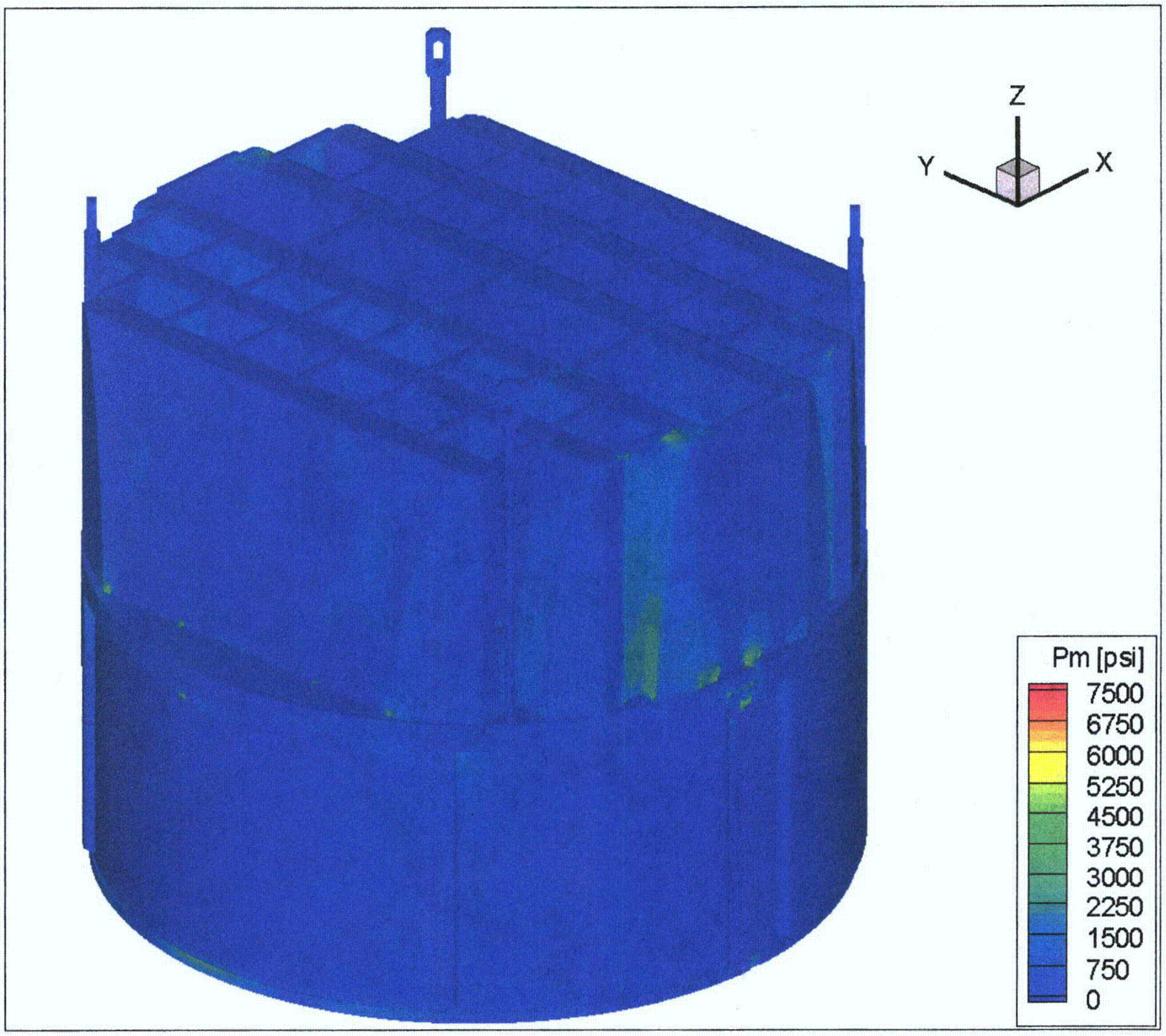

Figure 13a. Contour plot of maximum membrane stress intensity, Pm, for CLTP operation with frequency shifts. The recorded stress at a node is the maximum value taken over all frequency shifts. The maximum stress intensity is 7490 psi.

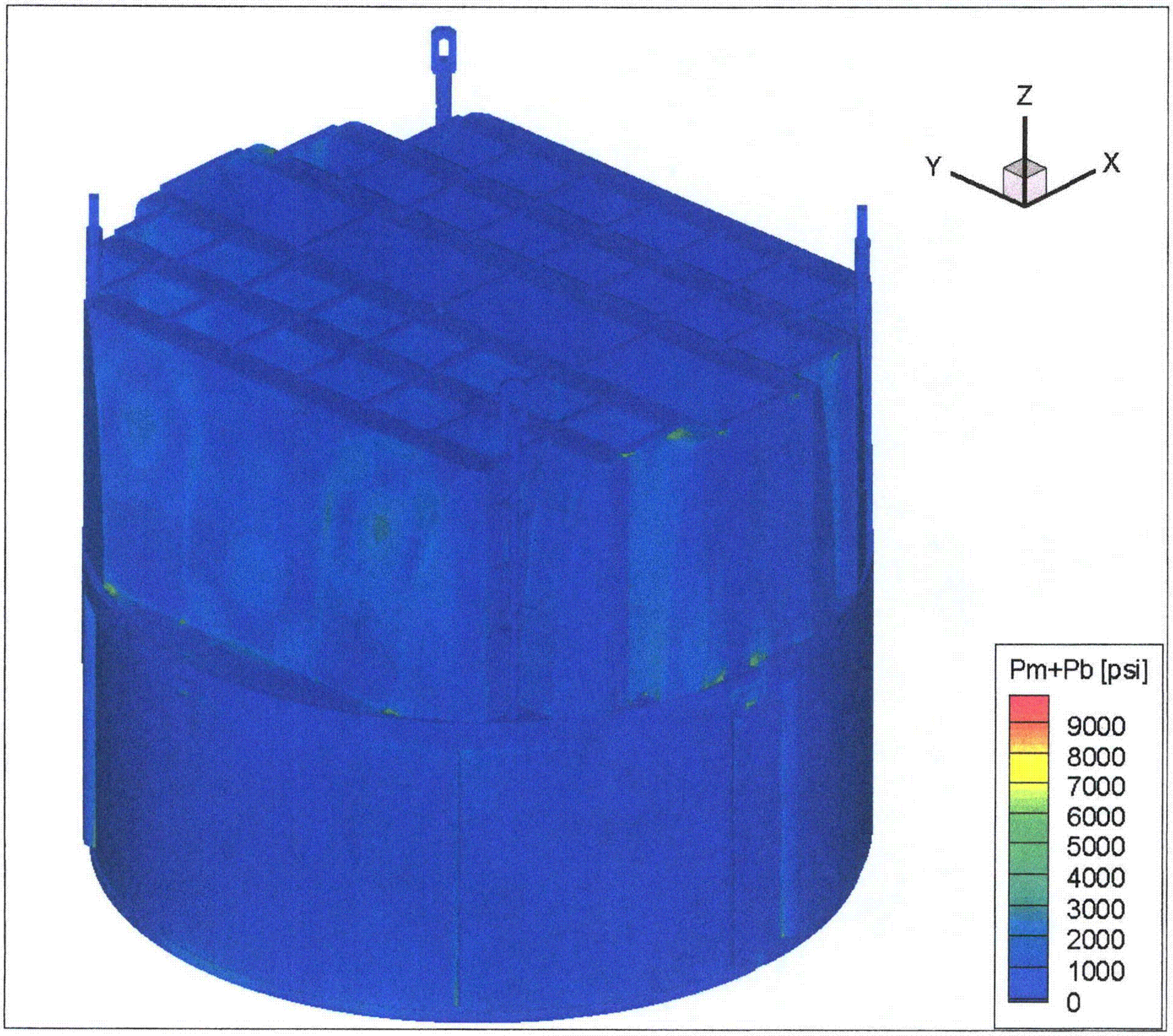

Figure 13b. Contour plot of maximum membrane+bending stress intensity, Pm+Pb, for CLTP operation with frequency shifts. The recorded stress at a node is the maximum value taken over all frequency shifts. The maximum stress intensity is 9809 psi. First view.

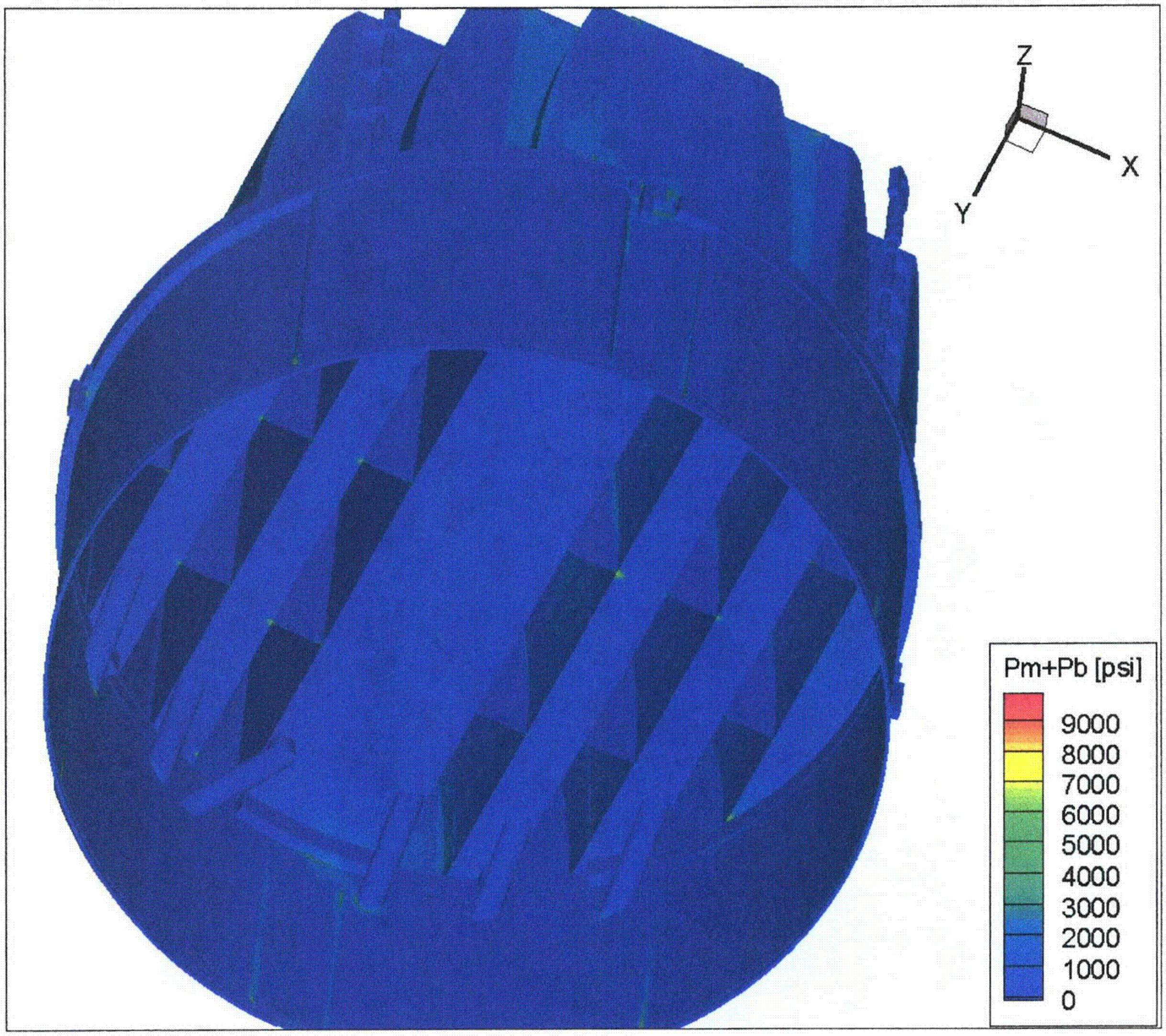

Figure 13c. Contour plot of maximum membrane+bending stress intensity, Pm+Pb, for CLTP operation with frequency shifts. This second view from beneath reveals stresses on the hood support/base plate junctions, outer cover plate and drain channel/skirt welds.

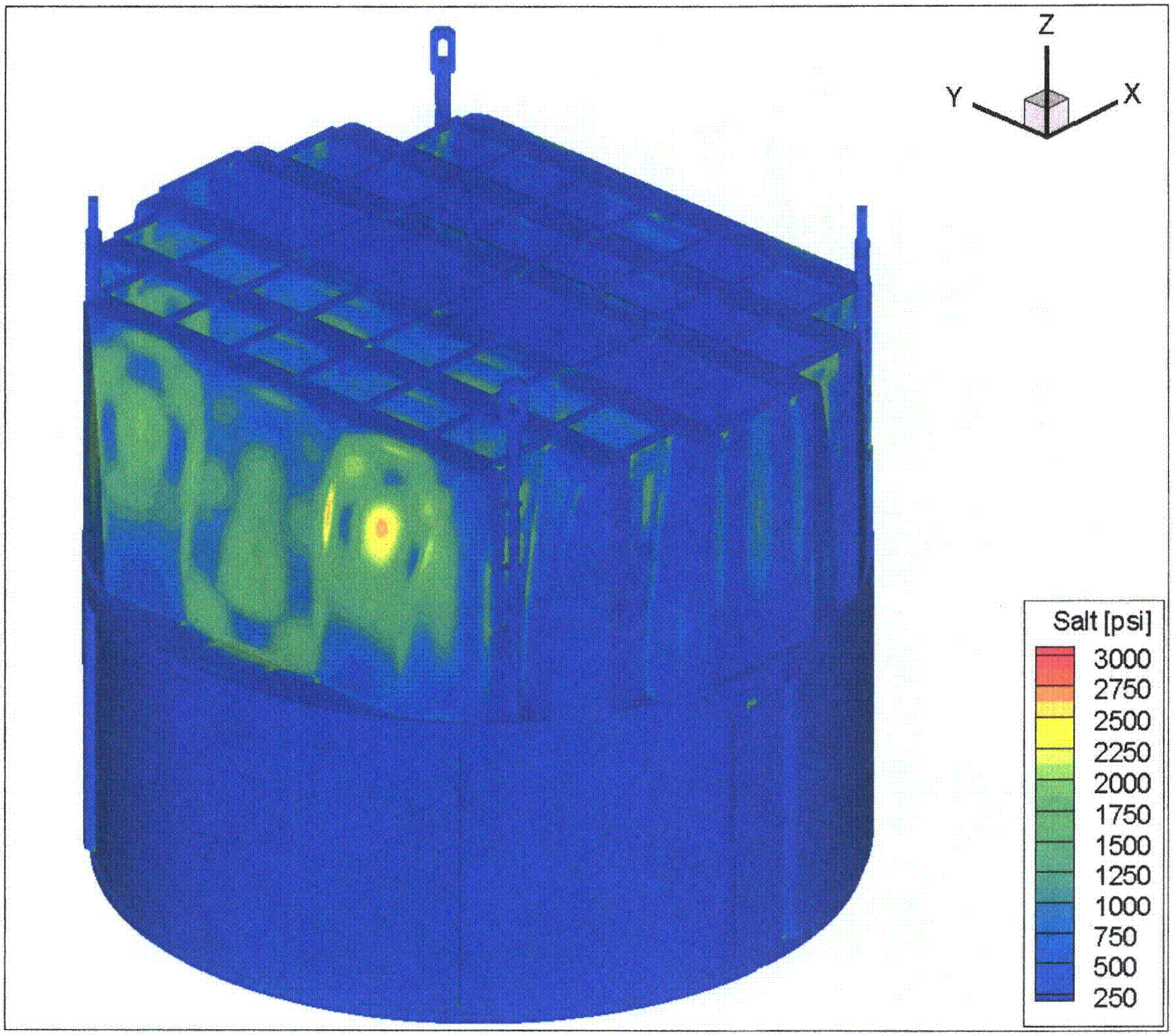

Figure 13d. Contour plot of alternating stress intensity, S_{alt}, for CLTP operation with frequency shifts. The recorded stress at a node is the maximum value taken over all frequency shifts. The maximum alternating stress intensity is 2914 psi. First view.

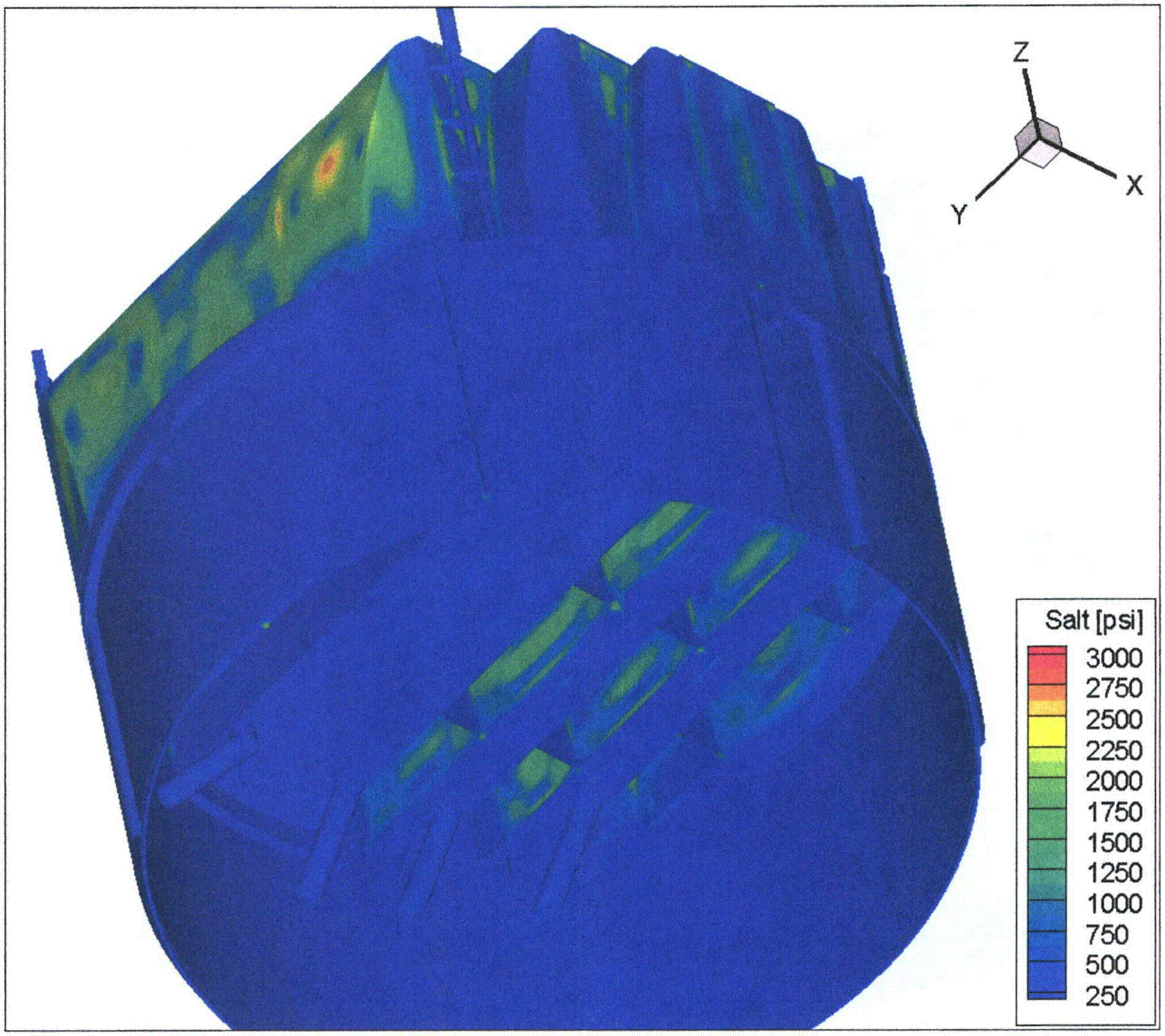

Figure 13e. Contour plot of alternating stress intensity, S_{alt}, for CLTP operation with frequency shifts. The recorded stress at a node is the maximum value taken over all frequency shifts. Second view from below.